Dalton Transactions

Identifying Charge-Transfer and Trip-Multiplet States in Co(I), Co(II), and Co(III) phthalocyanines using (magneto)optical spectroscopy and (TD)DFT calculations

Journal:	*Dalton Transactions*
Manuscript ID	DT-ART-03-2025-000628.R1
Article Type:	Paper
Date Submitted by the Author:	16-Apr-2025
Complete List of Authors:	Muldowney, Breanna; The University of Tennessee Knoxville, Department of Chemistry Nevonen, Dustin; The University of Tennessee Knoxville, Department of Chemistry Jeaydi, Towhidi ; University of Akron, Chemistry Ziegler, Christopher; University of Akron, Department of Chemistry McNicholas, Brendon; The University of Tennessee Knoxville College of Arts and Sciences, Chemistry Nemykin, Viktor; The University of Tennessee Knoxville, Department of Chemistry

Identifying Charge-Transfer and Trip-Multiplet States in Co(I), Co(II), and Co(III) Phthalocyanines Using (Magneto)Optical Spectroscopy and (TD)DFT Calculations.

Breanna E. Muldowney,[a] Dustin E. Nevonen,[a,b] Towhidi Illius Jeaydi,[c] Christopher J. Ziegler,*[c] Brendon J. McNicholas,*[a] and Victor N. Nemykin,*[a]

[a]*Department of Chemistry, University of Tennessee, Knoxville, Tennessee 37996, United States*

[b]*Department of Chemistry and Biochemistry, Wichita State University, Wichita, KS 67260, United States*

[c] *Department of Chemistry, University of Akron, Akron, Ohio 44325, United States*

Dedicated to the memory of Professor Barry Lever (A. B. P. Lever)

Abstract

Herein we compare the electronic structures of the Co(I), Co(II), and Co(III) phthalocyanines, which were elucidated using UV-vis-NIR and magnetic circular dichroism (MCD) spectroscopy as well as density functional theory (DFT) and time-dependent DFT (TDDFT) calculations. The NIR triplet-multiplet bands in $Pc^{R4}(2\text{-})Co^{II}L_2$ (L = nil, Py, or *n*$BuNH_2$; R = H or *tert*-Bu) complexes were studied by MCD spectroscopy for the first time and compared to those reported earlier by us in $Pc^{R4}(2\text{-})Cu$ (R = *tert*-Bu or SO_3Na) compounds (*J. Porphyrins Phthalocyanines* **2025**, *29*, 110-122). In all cases, a Faraday MCD pseudo *A*-term was observed for this transition. DFT and TDDFT calculations successfully explained a systematic blue-shift in the metal-to-ligand charge-transfer (MLCT) and B1-band transitions going from $[Pc^{R4}(2\text{-})Co^{I}]^-$ to $Pc^{R4}(2\text{-})Co^{II}L_2$ to $[Pc^{R4}(2\text{-})Co^{III}X_2]^-$ (X = CN^- or Br^-) complexes. Additionally, absorption bands observed in the 370-530 nm spectral envelope in $[Pc^{R4}(2\text{-})Co^{III}X_2]^-$ complexes were assigned with a high level of confidence for the first time. This work provides the first combined systematic experimental and theoretical study that highlights similarities and differences in (magneto)optical spectroscopy of cobalt phthalocyanines spanning three oxidation states at the central metal ion.

Introduction.

Transition-metal phthalocyanines are well-known blue or green pigments[1-3] that have many applications including catalysis,[4-15] photocatalysis,[16-20] electrocatalysis,[21-28] light-harvesting,[29-34] molecular electro- or chemochromic sensing,[35-40] photodynamic and catalytic cancer therapy,[41-47] semiconductors,[48-51] and fluorescence (bio)imaging.[52-54] In particular, cobalt phthalocyanine is known for its ability to oxidize thiols to disulfides (the so-called "Merox" process or jet fuel sweetening process).[55-62] During the catalytic cycle, the cobalt ion cycles between Co(III) and Co(I). The ability to characterize both metal-centered oxidation and reduction processes in cobalt phthalocyanine is well-documented, and a number of Co(III),[63-73] Co(II),[74-80] and Co(I)[81-85] phthalocyanine complexes coordinated to the Pc(2-) ligand have been isolated and characterized by a variety of experimental methods. Such ability is uncommon due to the redox non-innocence of the phthalocyanine ligand. Thus, taking into consideration the incomplete d-orbital subset in cobalt phthalocyanines, investigating these systems in a systematic way using optical and magnetooptical spectroscopy in combination with modern density functional theory (DFT) and time-dependent DFT (TDDFT) methods provides a unique opportunity to study the influence of the oxidation state at the central metal ion on the charge-transfer processes as well as phthalocyanine-centered π–π^* transitions in a systematic way (**Figure 1**).

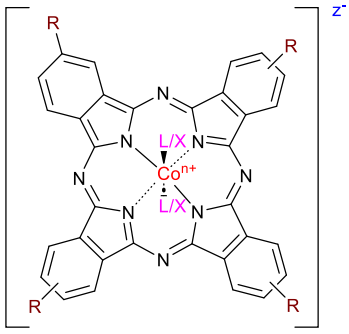

Complex	n	z	R	L	X
$[Pc(2-)Co^{I}]^-$	1	1	H	none	none
$Pc^{tBu}(2-)Co^{II}$	2	0	tBu	none	none
$Pc(2-)Co^{II}Py_2$	2	0	H	Py	none
$Pc^{tBu}(2-)Co^{II}Py_2$	2	0	tBu	Py	none
$Pc(2-)Co^{II}(n\text{BuNH}_2)_2$	2	0	H	$n\text{BuNH}_2$	none
$Pc^{tBu}(2-)Co^{II}(n\text{BuNH}_2)_2$	2	0	tBu	$n\text{BuNH}_2$	none
$[Pc(2-)Co^{III}(CN)_2]^-$	3	1	H	none	CN^-
$[Pc^{tBu}(2-)Co^{III}Br_2]^-$	3	1	tBu	none	Br^-

Figure 1. General structure of the phthalocyanines and systems discussed in this report.

In particular, the d^6-d^8 electronic configurations in Co(III)-Co(I) phthalocyanine systems allow us to study the trends in energies of the d_π(Co) → $1b_{1u}$*, $1b_{2u}$* (Pc) metal-to-ligand charge-transfer (MLCT) transitions. In addition, Co(II) (but not Co(III) or Co(I)) phthalocyanine complexes have a weak set of bands observed in the NIR region of their UV-Vis-NIR spectra. These bands were initially assigned as d-d transitions.[86-89] However, Lever and co-workers assigned these bands as triplet-multiplet (*t-m*) transitions.[90] Zerner and Cory introduced the theory of *t-m* transitions for paramagnetic porphyrins and their analogs in the early 1990s.[91] Indeed, although singlet-triplet transitions in diamagnetic transition-metal phthalocyanines are spin-forbidden, Ishii and co-workers observed such a transition in $Pc^{tBu}(2-)Ir^{III}Cl(Py)$ at 959 nm.[92] Similar to the Q-band, this transition is degenerate (**Figure 2a**) and results in a weak but observable Faraday *A*-term by magnetic circular dichroism (MCD) spectroscopy.

In the case of paramagnetic transition-metal phthalocyanines, a metal-ligand exchange can provide a path for spin-allowed *t-m* transitions that include a triplet state at the phthalocyanine ligand (**Figure 2b**; see original paper by Cory and Zerner[91] for detailed discussion). In triplet-multiplet transition, the organic chromophore (i.e., phthalocyanine) goes from the singlet state to a triplet state, while the multiplicity of the transition-metal phthalocyanine remains the same (i.e. doublet in the case of cobalt(II) phthalocyanines, Figure 2b).[91] Again, such an excited state will be doubly degenerate for all paramagnetic transition-metal phthalocyanines with the effective D_{4h} or C_{4v} symmetry and thus should be associated with a Faraday *A*-term in their MCD spectra, unless a complex possesses a doubly degenerate ground state (i.e. $[Pc(2-)Fe^{III}(CN)_2]^-$ has a ^2E_g ground state), which will have both Q- and *t-m* transitions better described using Faraday C_A-terms.[93] Indeed, we recently observed Faraday *A*-terms for the *t-m* transitions in two copper(II) phthalocyanines.[94] Moreover, since both singlet-singlet Pc-centered ligand excitations lead to the traditional phthalocyanine Q-band (**Figure 2c**) and phthalocyanine-centered singlet-triplet excitations (**Figure 2b**) exhibit nearly pure $1a_{1u} \rightarrow 1e_g^*$ single-electron character, one might expect that the Q- and *t-m* bands will exhibit similar vibronic progression components. Again, we reported this phenomenon for copper(II) phthalocyanines.[94] Thus, investigation of the NIR absorption and MCD spectra in paramagnetic (s = ½) Co(II) phthalocyanines should resolve the ambiguous NIR band assignments for d-d and *t-m* transitions. Because of the increased tendency towards aggregation and lower solubility of unsubstituted phthalocyanines, we used a highly soluble, less aggregating *tert*-butyl substituted phthalocyanine core as it is well-known[95-97] that the introduction of the *tert*-butyl groups into the phthalocyanine chromophore does not significantly change its optical properties (**Figure 1**). Finally, as we demonstrated for copper(II) and vanadyl(IV) phthalocyanines,[94] TDDFT calculations are able to accurately predict the energies of

t-m transitions, allowing us to solidify proposed band assignments in the NIR region for $Pc^{R4}(2-)Co^{II}L_2$ (R = H or *tert*-Bu; L = nil, Py, or nBuNH$_2$).

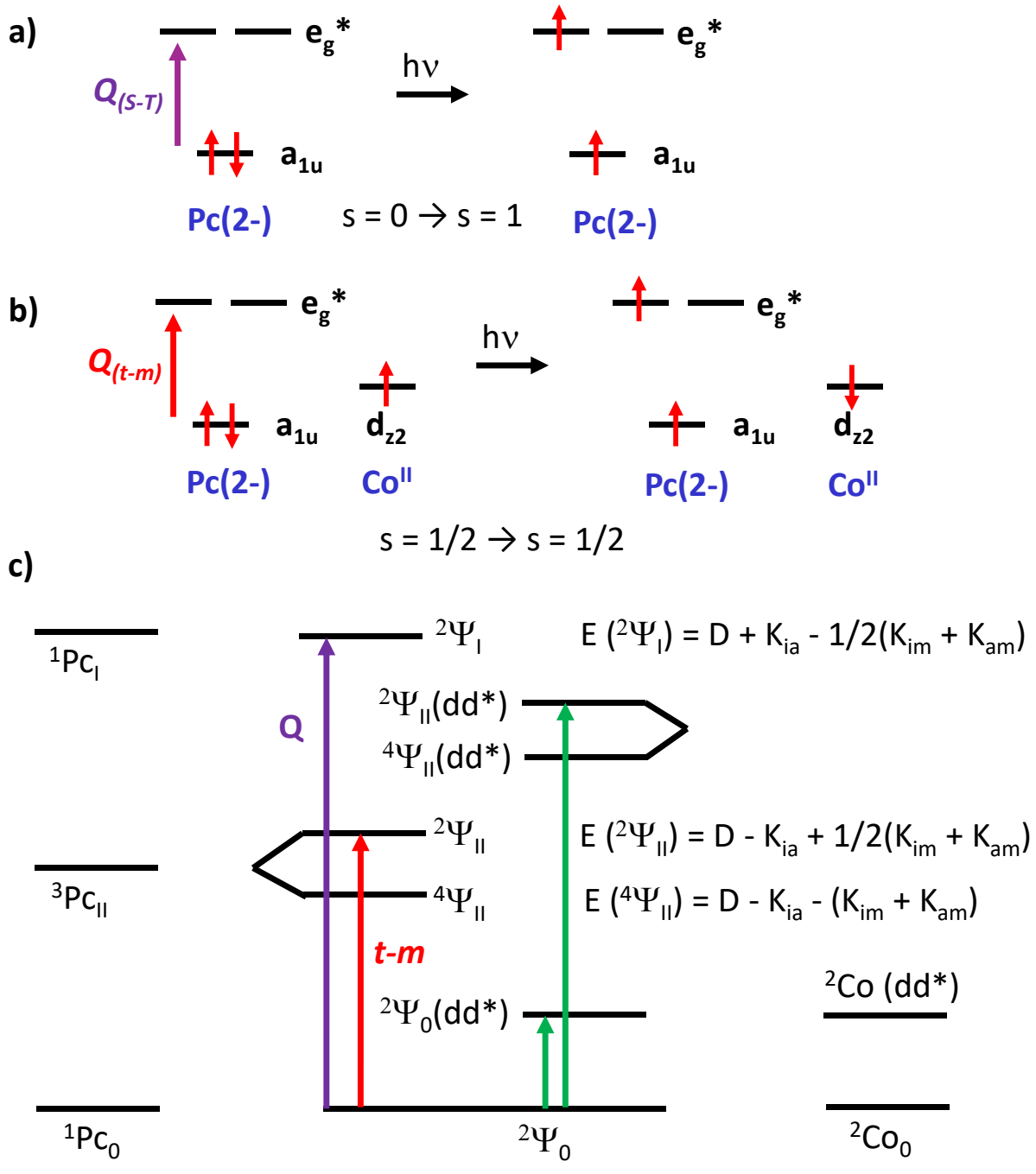

Figure 2. Simplified illustration of the singlet-triplet (a) and triplet-multiplet (b) transitions. Simplified representation of the excited states in the low-energy region of the cobalt(II) (s = ½) phthalocyanine systems (c). The energies of the selected transitions are given on a side panel (K_{ia} is an exchange integral between occupied and virtual orbitals in the phthalocyanine ligand; K_{im} is an exchange integral between occupied orbitals in the phthalocyanine ligand and cobalt(II) center; K_{am} is an exchange integral between unoccupied orbitals in the phthalocyanine ligand and cobalt(II) center; D is an offset energy).[91]

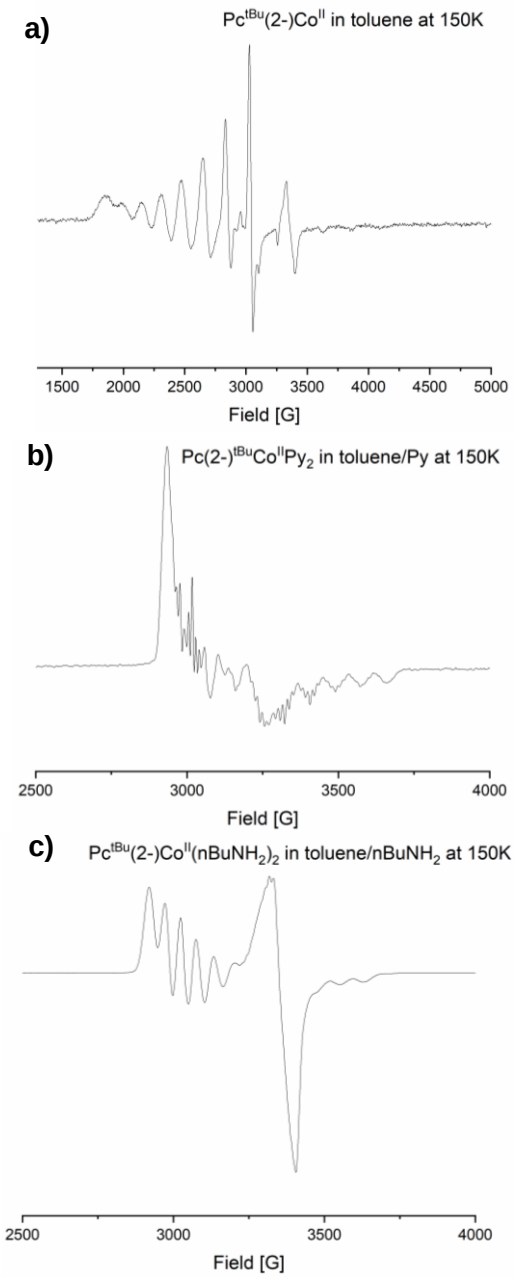

Figure 3. 150 K EPR spectra of the $Pc^{tBu}(2\text{-})Co^{II}$ complex in toluene (a), $Pc^{tBu}(2\text{-})Co^{II}Py_2$ complex in 95/5% (v/v) toluene/pyridine (b), and $Pc^{tBu}(2\text{-})Co^{II}(n\text{BuNH}_2)_2$ complex in 95/5% (v/v) toluene/$n\text{BuNH}_2$ (c).

Results and Discussion

The cobalt(I-III) phthalocyanine derivatives discussed in this paper are shown in **Figure 1**. Synthetic procedures for all cobalt phthalocyanines outlined in this report are well-developed except for $[Pc^{tBu}(2\text{-})Co^{III}Br_2]^-$. Indeed, diamagnetic $[Pc^{R4}(2\text{-})Co^{I}]^-$ complexes can be prepared by the reduction of $Pc^{R4}(2\text{-})Co^{II}$ with $NaBH_4$ in DMF.[98,99] Axially coordinated $Pc^{R4}(2\text{-})Co^{II}L_2$ (L = Py or $nBuNH_2$) can be synthesized by the reaction of $Pc^{R4}(2\text{-})Co^{II}$ and excess ligand.[74-80] Coordination of two axial ligands in these compounds was confirmed by both UV-Vis spectroscopy and EPR spectroscopy (**Figure 3**, **Table 1**). Indeed, EPR spectra of the $Pc^{tBu}(2\text{-})Co^{II}$, $Pc^{tBu}(2\text{-})Co^{II}Py_2$, and $Pc^{tBu}(2\text{-})Co^{II}(n\text{BuNH}_2)_2$ complexes correlate well with EPR spectra previously published by Larin and co-workers[101,102] for *tert*-butyl- and by Cariati and co-workers[86,87] for unsubstituted phthalocyanine ligands. Additionally, coordination of two pyridine ligands as well as a low-spin $(d_{xy})^2(d_{xz},d_{yz})^4(d_{z2})^1$ electronic configuration in $Pc^{tBu}(2\text{-})Co^{II}Py_2$ complex can be proven by observation of five-line superhyperfine splitting in its EPR spectrum (**Figure 3**).[101,102] Simple addition of cyanide anion to a solution of $Pc(2\text{-})Co^{II}$ in DMF leads to axial coordination and destabilization of the d_{z2} orbital, making it easier for oxygen to oxidize the central metal ion to diamagnetic Co(III) upon the formation of $[Pc(2\text{-})Co^{III}(CN)_2]^-$.[72,73,103] Synthesis of the $[Pc(2\text{-})Co^{III}Br_2]^-$ complex was reported by Homberg and co-authors.[71] It involves the preparation of $[Pc(1\text{-})Co^{III}(TFA)]^+$ cation (TFA = trifluoroacetate) and its interaction with HBr. We found that $[Pc^{tBu}(2\text{-})Co^{III}Br_2]^-$ can be prepared in two different ways. First, a simple electrochemical oxidation of $Pc^{tBu}(2\text{-})Co^{II}$ in the DCM / 0.3 M TBABr system leads to the formation of $[Pc^{tBu}(2\text{-})Co^{III}Br_2]^-$ (**Figure 4a**). Thus, one can use bulk electrolysis to synthesize this compound. Electrochemical oxidation allowed us to develop a more convenient way of preparing $[Pc^{tBu}(2\text{-})Co^{III}Br_2]^-$. Indeed,

oxidation of [Pc^{tBu}(2-)Co^{II}] in DCM / 0.3M TBABr with a solution of bromine in DCM results in the clean formation of [Pc^{tBu}(2-)$Co^{III}Br_2$]$^-$ suitable for spectroscopic studies (**Figure 4b**).

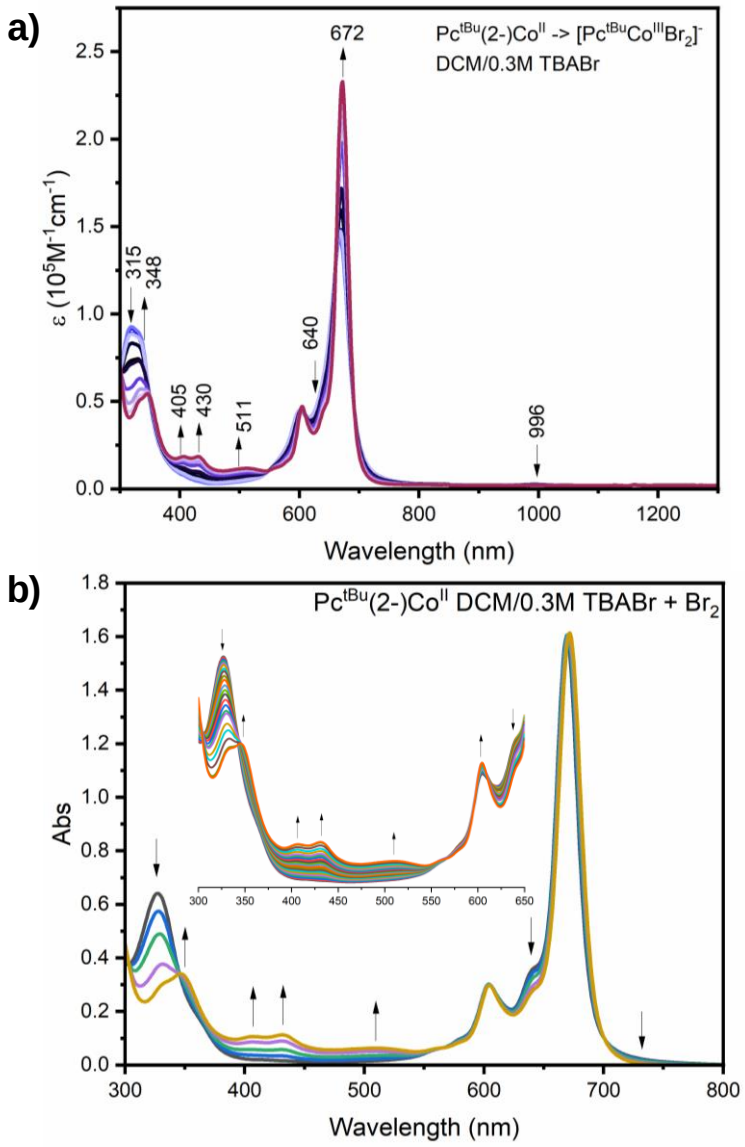

Figure 4. Formation of [$Pc^{tBu}Co^{III}Br_2$]$^-$ under spectroelectrochemical oxidation conditions in DCM / 0.3 M TBABr (a) and under chemical oxidation conditions using bromine as an oxidant in the same solvent system (b).

Table 1. EPR parameters for selected cobalt(II) phthalocyanines.

Compound	$g_{\parallel}$	$g_{\perp}$	$a_{\parallel}^{Co}$, cm^{-1}	$a_{\perp}^{Co}$, cm^{-1}	$a_{\parallel}^{N}$, cm^{-1}	$a_{\perp}^{N}$, cm^{-1}	Ref.
$Pc^{tBu}(2\text{-})Co^{II}$	1.945	2.677	149.9	195.5			101[a]
	1.95	2.78	150	190			*tw*[d]
Pc(2-)Co^{II} /calc.	*2.004*	*2.314*	*195*	*31*			*tw*
β-$Pc(2\text{-})Co^{II}$	1.89	2.94	150	280			104[b]
α-$Pc(2\text{-})Co^{II}$	1.99	2.60	110	64			104[b]
$Pc^{tBu}(2\text{-})Co^{II}Py_2$	2.013	2.250	75.2		15	11	101[a]
	2.01	2.21	85		14	10	*tw*[e]
Pc(2-)Co^{II}Py$_2$ /calc.	*1.994*	*2.155*	*113*	*61*			*tw*
$Pc(2\text{-})Co^{II}(4\text{-MePy})_2$	2.015	2.25	77	12	14		86[c]
$Pc^{tBu}(2\text{-})Co^{II}(n\text{BuNH}_2)_2$	2.01	2.18		53			*tw*[f]
Pc(2-)Co^{II}(nBuNH$_2$)$_2$ /calc.	*1.991*	*2.136, 2.135*	*76*	*102*			*tw*
$Pc^{tBu}(2\text{-})Co^{II}(i\text{BuNH}_2)_2$	2.011	2.186	70.4	57.5	14.5		101[a]

[a] 77 K, PhMe; [b] diluted with PcZn; [c] 4-MePy/DCM (70/30, v/v) 77 K; [d] 150 K PhMe, *tw* = this work; [e] 150K Py/PhMe (5/95, v/v); [f] 150 K *n*$BuNH_2$/PhMe (5/95, v/v).

Formation of square planar $Pc(2\text{-})Co^{II}$ [105] and $[Pc(2\text{-})Co^{I}]^{-}$ [100,106] as well as tetragonally distorted $[Pc(2\text{-})Co^{III}(CN)_2]^{-}$,[65,107-109] $[Pc(2\text{-})Co^{III}Br_2]^{-}$,[71] and $Pc(2\text{-})Co^{II}Py_2$[110,111] was confirmed by X-ray crystallography in previous reports. The UV-Vis-NIR and MCD spectra of $[Pc(2\text{-})Co^{I}]^{-}$, $[Pc^{tBu}(2\text{-})Co^{I}]^{-}$, $Pc^{tBu}(2\text{-})Co^{II}$, $Pc(2\text{-})Co^{II}Py_2$, $Pc^{tBu}(2\text{-})Co^{II}Py_2$, $Pc(2\text{-})Co^{II}(n\text{BuNH}_2)_2$, Pc^{tBu}(2-

)Co^{II}(nBuNH$_2$)$_2$, [Pc(2-)Co^{III}(CN)$_2$]$^-$, and [Pc^{tBu}(2-)Co^{III}Br$_2$]$^-$ are grouped by the oxidation state of the central metal ion and shown in Figures 5-7 and Supporting Information Figure S1-4.

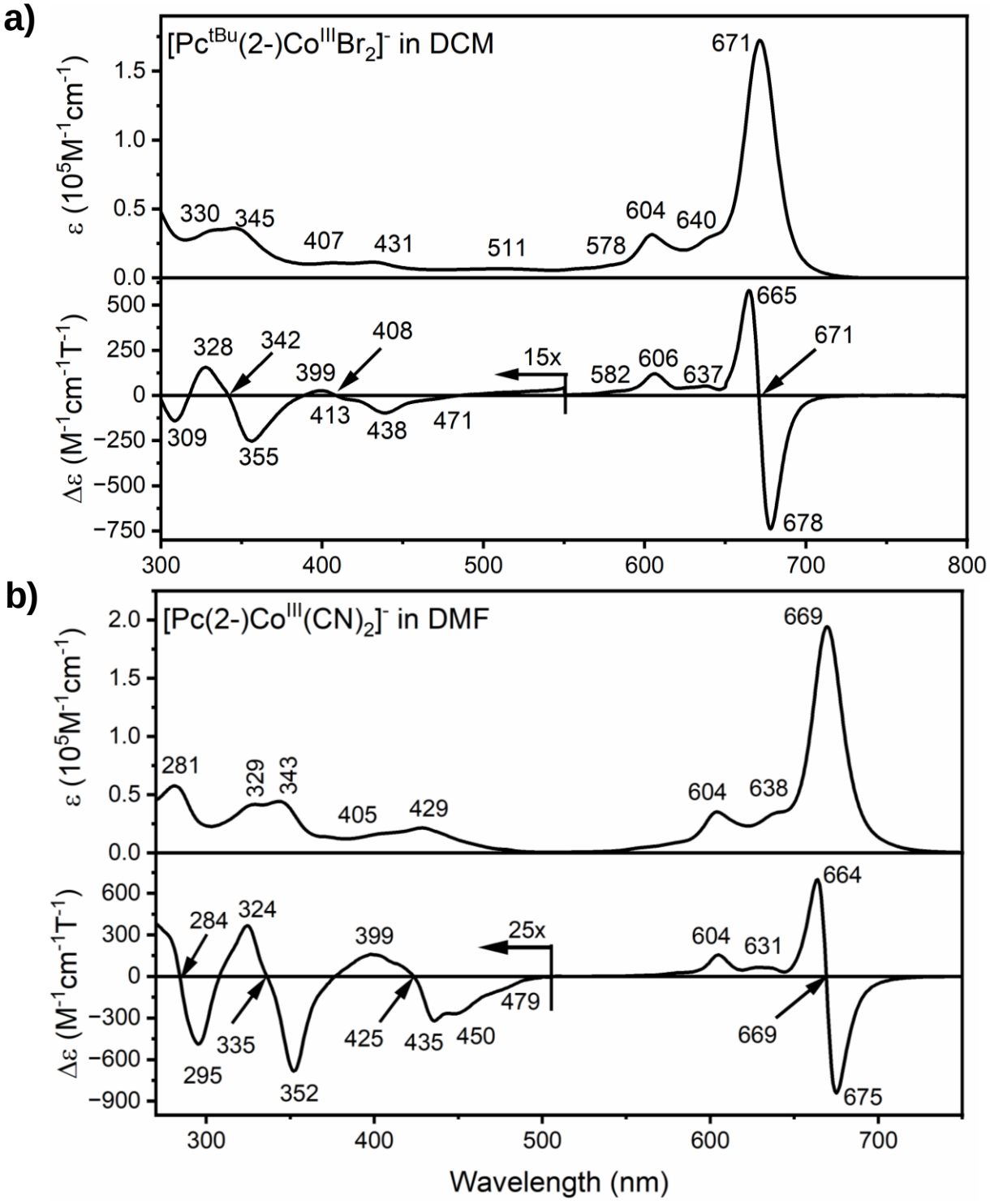

Figure 5. UV-Vis and MCD spectra of $[Pc^{tBu}(2\text{-})CoIIIBr2]^-$ in DCM (a) and $[Pc(2\text{-})Co^{III}(CN)_2]^-$ in DMF.

For cobalt(III) derivatives, in addition to the Q-bands and their vibronic satellites observed in the 550-700 nm region and split B-bands observed in the 300-350 nm region, additional transitions were detected between 400 and 550 nm (**Figure 5**). Specifically, bands at 429 and 405 nm were detected for the $[Pc(2\text{-})Co^{III}(CN)_2]^-$ complex. The transition at 429 nm is associated with a MCD Faraday *A*-term centered at 425 nm. However, in addition to this *A*-term, two visible shoulders with a negative amplitude were observed at 450 and 479 nm followed by an MCD signal with a positive amplitude at 399 nm (**Figure 5**). Two additional visible Faraday *A*-terms observed at 335 and 284 nm are associated with the absorption bands observed at 343 and 281 nm. In the case of the UV-Vis spectrum of the $[Pc^{tBu}(2\text{-})Co^{III}Br_2]^-$ complex (which is indistinguishable from the UV-Vis spectrum of $[Pc(2\text{-})Co^{III}Br_2]^-$ published by Homborg and co-workers),[71] additional bands at 511, 431, and 407 nm were observed. The low-energy band at 511 nm is not associated with a clear MCD signal, while the absorption band at 431 nm is associated with a Faraday *B*-term of negative amplitude centered at 438 nm along with a shoulder at 471 nm. The absorption band at 407 nm is associated with a MCD *A*-term centered at 408 nm. These signals are better separated than the bands observed for the $[Pc(2\text{-})Co^{III}(CN)_2]^-$ complex in the same spectral envelope. As expected, the MCD spectra of both cobalt(III) complexes are dominated by a very strong Faraday *A*-term associated with the $Q_{0\text{-}0}$ transition. No signals were detected for both cobalt(III) systems with energies lower than the energy of the $Q_{0\text{-}0}$ transition.

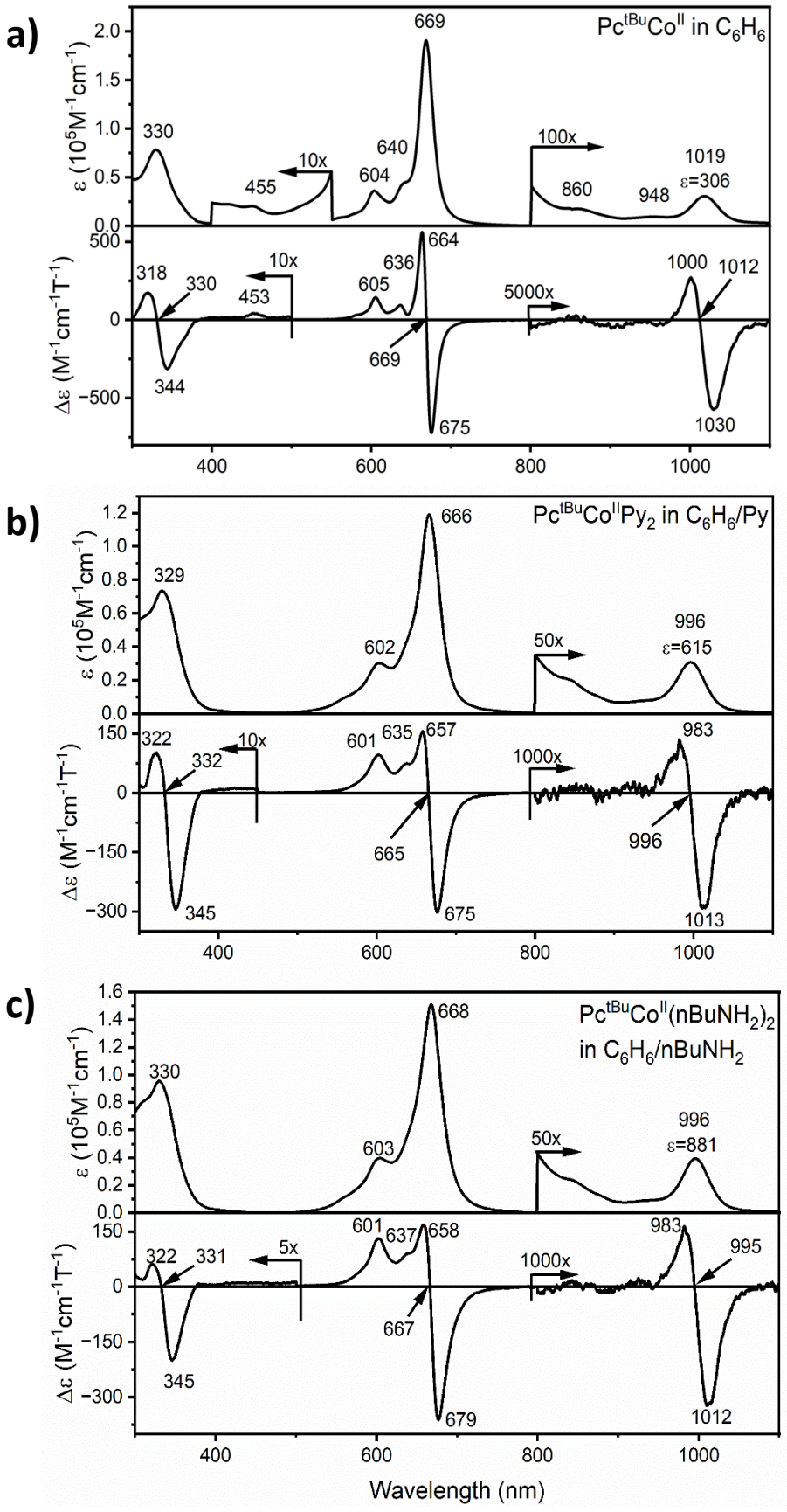
a)
$Pc^{tBu}Co^{II}$ in C_6H_6
ε ($10^5 M^{-1}cm^{-1}$)
Δε ($M^{-1}cm^{-1}T^{-1}$)
669
330
640
604
455
10x
100x
860
948
1019
ε=306
318
330
453
636
605
664
5000x
1000
1012
344
669
675
1030
b)
$Pc^{tBu}Co^{II}Py_2$ in C_6H_6/Py
666
329
602
50x
996
ε=615
322
332
601
635
657
1000x
983
665
996
345
675
1013
c)
$Pc^{tBu}Co^{II}(nBuNH_2)_2$
in C_6H_6/$nBuNH_2$
668
330
603
50x
996
ε=881
322
331
5x
601
637
658
1000x
983
995
345
667
679
1012
400
600
800
1000
Wavelength (nm)

Figure 6. UV-Vis and MCD spectra of $Pc^{tBu}(2\text{-})Co^{II}$ in benzene (a), $Pc^{tBu}(2\text{-})Co^{II}Py_2$ in benzene/pyridine (95/5%, b), and $Pc^{tBu}(2\text{-})Co^{II}(n\text{BuNH}_2)_2$ in benzene/nBuNH$_2$ (95/5%, c).

$Pc(2\text{-})Co^{II}Py_2$ and $Pc(2\text{-})Co^{II}(n\text{BuNH}_2)_2$ were studied first for cobalt(II) derivatives. In both cases, spectra were dominated by absorption in the Q- and B-band regions (Supporting Information Figure S3 and S4). The Q-band is associated with a strong MCD *A*-term centered close to the absorption maxima. The MCD spectra in the B-band region are indicative of several transitions present in this spectral envelope. Additionally, a series of low-energy, low-intensity bands between 800 and 1000 nm was observed in both cases. These were previously assigned as d-d[86-89] or *t*-*m*[90] transitions, and their nature will be discussed in detail in the next section. The lowest energy band in the NIR region is associated with an MCD *A*-term (Supporting Information Figure S3 and S4). However, because of the limited solubility and pronounced aggregation at higher concentrations of the $Pc(2\text{-})Co^{II}Py_2$ and $Pc(2\text{-})Co^{II}(n\text{BuNH}_2)_2$ complexes with unsubstituted phthalocyanine cores, we were not able to obtain a well-resolved spectroscopic signature in the MCD spectra for the bands observed between 940 and 810 nm. Moreover, the parent $Pc(2\text{-})Co^{II}$ has limited solubility in non-coordinating solvents that are transparent between 270 and 1000 nm. Thus, we moved to *tert*-butyl substituted phthalocyanine derivatives to overcome these problems. UV-Vis-NIR and MCD spectra of $Pc^{tBu}(2\text{-})Co^{II}$, $Pc^{tBu}(2\text{-})Co^{II}Py_2$, and $Pc^{tBu}(2\text{-})Co^{II}(n\text{BuNH}_2)_2$ complexes are shown in **Figure 6**. These closely follow the spectra of the unsubstituted $Pc(2\text{-})Co^{II}Py_2$ and $Pc(2\text{-})Co^{II}(n\text{BuNH}_2)_2$ derivatives. The vibronic satellites in the UV-Vis-NIR and MCD spectra of $Pc^{tBu}(2\text{-})Co^{II}$ in the Q-band region are much better resolved, with the $Q_{0\text{-}0}$ transition being significantly narrower compared to the $Q_{0\text{-}0}$ transitions in $Pc^{tBu}(2\text{-})Co^{II}Py_2$ and $Pc^{tBu}(2\text{-})Co^{II}(n\text{BuNH}_2)_2$ complexes. The broader $Q_{0\text{-}0}$ bands in $Pc^{tBu}(2\text{-})Co^{II}Py_2$ and

$Pc^{tBu}(2\text{-})Co^{II}(n\text{BuNH}_2)_2$ complexes can be explained with the equilibria between hexa-, penta-. and tetra-coordinated complexes in solution (i.e., $Pc^{R4}(2\text{-})Co^{II}L_2 \rightleftarrows Pc^{R4}(2\text{-})Co^{II}L + L \rightleftarrows Pc^{R4}(2\text{-})Co^{II} + L$).[74-80] Next, because we were able to increase the concentrations of *tert*-butyl derivatives, we obtained improved resolution of the transitions observed in the NIR region both in the absorption and MCD spectra. Similar to the $Pc(2\text{-})Fe^{II}L_2$ complexes reported previously,[112] the nature of the solvent and the coordination of axial ligands have a very minor influence on the energy of the $Q_{0\text{-}0}$ band. The same is true for the lowest-energy band observed in the NIR region. The lowest energy NIR band is associated with a MCD *A*-term, confirming the degenerate nature of this excited state.

Finally, the UV-Vis and MCD spectra of the $[Pc^{R4}(2\text{-})Co^{I}]^-$ anion have very rich spectroscopic signatures between 400 and 600 nm (**Figure 7** and Supporting Information Figures S1 and S2). There are at least three MCD *A*-terms visible in this spectral envelope located at ~430, ~475, and ~530 nm (**Figure 7**). The two most intense bands are associated with the absorption bands at 428 nm and 469 nm. However, both UV-Vis and MCD spectra are indicative of the presence of a larger number of transitions in this region. In particular, the Faraday *A*-term at ~530 nm and the *B*-term at ~545 nm are associated with shoulders at 519 and 556 nm observed in the UV-Vis spectrum of $[Pc^{R4}(2\text{-})Co^{I}]^-$. Stillman and Thomson suggested that the B-band in $[Pc(2\text{-})Co^{I}]^-$ should be observed in the 400-500 nm region,[98] while Lever indicated that MLCT transitions should be present in this spectral envelope.[113] The $Q_{0\text{-}0}$ band is red-shifted compared to those in cobalt(III) and cobalt(II) derivatives. There is also a strong MCD *B*-term at ~630 nm with positive amplitude present in the spectrum of the $[Pc(2\text{-})Co^{I}]^-$ anion (Supporting Information Figure S1). This MCD *B*-term is close to but not perfectly aligned with the absorption band at 637 nm observed in the UV-Vis spectrum of $[Pc(2\text{-})Co^{I}]^-$. Interestingly, the positive amplitude component of the *A*-term associated with the $Q_{0\text{-}0}$ band in the $[Pc(2\text{-})Co^{I}]^-$ anion has significantly lower intensity

compared to the negative amplitude component of the same transition. This could be reflective of the aggregation of $[Pc(2-)Co^{I}]^{-}$ in DMF. Indeed, it is well-known that phthalocyanine H-aggregates,[114-117] cofacial μ-oxo dimers,[118-122] and double-decker systems[123-128] have blue-shifted Q_{0-0}-bands and exhibit MCD *A*-terms. If both the monomer and H-aggregate of the $[Pc(2-)Co^{I}]^{-}$ anion are present in solution, then the positive amplitude component of the *A*-term in the monomer will be reduced because of the negative component of the *A*-term of the H-aggregate (Supporting Information Figure S5). When *tert*-butyl substituted $[Pc^{tBu}(2-)Co^{I}]^{-}$ was studied by MCD spectroscopy in DMF (Supporting Information Figure 2) and THF (**Figure 7**), the Q_{0-0} band was observed as a more symmetric *A*-term and the amplitude of the band associated with the H-aggregate was significantly reduced (we should note that the *A*-term of the H-aggregate should overlap with the Q_{0-2} band and thus, the positive amplitude signal in ~630 nm region should not completely disappear). As expected for the low spin, diamagnetic d^8 system, no weak NIR absorption bands were observed in the UV-Vis-NIR and MCD spectra of $[Pc(2-)Co^{I}]^{-}$.

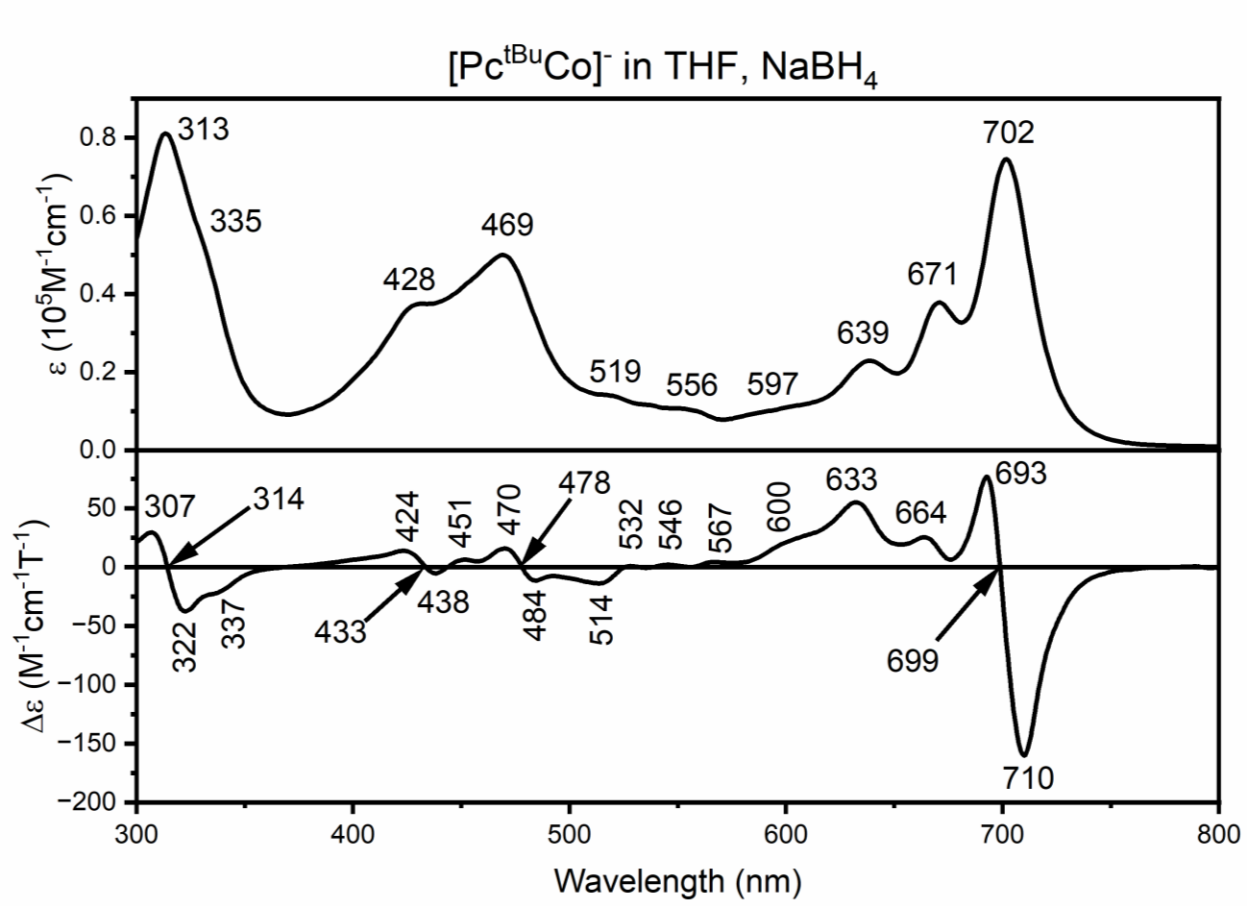

Figure 7. UV-Vis and MCD spectra of $[Pc^{tBu}(2\text{-})Co^{I}]^-$ in THF.

Analysis of the excited states in cobalt phthalocyanine complexes using DFT and TDDFT calculations.

The MCD spectra of $[Pc(2\text{-})Co^{III}(CN)_2]^-$, $Pc(2\text{-})Co^{II}Py_2$, and $[Pc(2\text{-})Co^{I}]^-$ complexes in the UV-Vis region between ~270 and 800 nm were first reported by Thomson and Stillman in their pioneering work in 1974.[98] These are consistent with our data. Understandably, the only spectral interpretation the authors were able to provide at that time was based on general ligand-field theory considerations and comparison with the spectra of closed-shell zinc(II) and iron(II) derivatives.

Based on these considerations, Thomson and Stillman suggested that the MCD *A*-term observed between ~400-470 nm for $[Pc(2-)Co^{I}]^{-}$ belongs to the B1 band.[98] Beyond these initial studies, several MCD spectra of substituted $Pc^{Rn}(2-)Co^{II}Py_2$ complexes were published through the years.[75-80] In the middle of the 1980s, Lever and co-authors attempted to analyze the energies of the charge-transfer states in phthalocyanine cobalt complexes based on their electrochemical reduction and oxidation potentials.[113] This analysis led to the conclusion that at least some charge-transfer transitions should be present between 400 and 500 nm for $[Pc(2-)Co^{I}]^{-}$.

Table 2. DFT-predicted molecular orbital compositions for diamagnetic cobalt(III) and cobalt(I) complexes;[a]

$[Pc(2-)Co^{III}(Br)_2]^{-}$					
MO	E, eV	Symm	Pc	Co	Br
191	-0.043	a_{1g}	5.19	93.26	1.56
190, 189	-1.151	e_g	99.15	0.68	0.17
188	-1.155	a_{2u}	96.81	1.35	1.84
187	-1.462	b_{2u}	99.99	0.00	0.01
186	-1.619	b_{1u}	100	0.00	0.00
185	-2.159	b_{1g}	55.54	44.46	0.00
184, 183	-3.118	e_g	97.52	1.76	0.72
182	***-3.287***	***a_{1g}***	***16.82***	***42.74***	***40.43***
181	***-4.995***	***a_{1u}***	***100***	***0.00***	***0.00***
180	-6.160	a_{2u}	57.11	1.30	41.58
179, 178	-6.267	e_g	20.48	2.39	77.14
177, 176	-6.302	e_g	45.69	41.99	12.32
175, 174	-6.579	e_u	15.72	1.88	82.4
173	-6.670	b_{2u}	99.99	0.00	0.01
172	-6.707	b_{2g}	75.56	24.44	0.00
171	-6.769	a_{2u}	99.39	0.16	0.45

170, 169	-6.868	e_g	99.76	0.07	0.17
168	-6.889	b_{1u}	100	0.00	0.00

$[Pc(2-)Co^{III}(CN)_2]^-$

MO	E, eV	Symm	Pc	Co	CN
168	-1.151	a_{2u}	97.36	0.444	2.20
166, 167	-1.193	e_g	98.91	0.860	0.24
165	-1.500	b_{2u}	100	0.00	0.00
164	-1.673	b_{1u}	100	0.00	0.00
163	-1.832	a_{1g}	24.18	41.11	34.71
162	-2.365	b_{1g}	54.91	45.09	0.00
160, 161	***-3.205***	***e_g***	***97.54***	***2.08***	***0.38***
159	***-5.056***	***a_{1u}***	***100***	***0.00***	***0.00***
158	-6.213	a_{2u}	70.15	1.06	28.79
157, 156	-6.378	e_g	66.65	32.3	1.04
155	-6.713	b_{2u}	100	0.00	0.00
154	-6.80	b_{2g}	78.94	21.06	0.00
153	-6.805	a_{2u}	99.29	0.14	0.57
152, 151	-6.898	e_g	99.11	0.51	0.38
150	-6.920	b_{1u}	100	0.00	0.00

$[Pc(2-)Co^{I}]^-$

MO	E, eV	Symm	Pc	Co
154	-0.548	b_{1g}	57.62	42.38
153, 152	-0.919	e_g	98.62	1.38
151	-1.050	a_{2u}	97.64	2.36
150	-1.253	b_{2u}	100	0.00
149	-1.355	b_{1u}	100	0.00
148, 147	***-2.624***	***e_g***	***87.08***	***12.92***
146, 145	***-4.490***	***e_g***	***35.06***	***64.94***
144	-4.504	a_{1g}	2.96	97.04
143	-4.691	a_{1u}	100	0.00
142	-5.572	b_{2g}	36.23	63.77

141	-6.388	b_{2u}	100	0.00
140	-6.484	a_{2u}	99.73	0.27
139, 138	-6.644	e_g	99.88	0.12
137	-6.675	b_{1u}	100	0.00
136	-6.709	a_{2u}	98.1	1.9

[a)] All complexes have D_{4h} symmetry; the frontier orbitals are formatted in bold. The C^2 method was used to calculate contributions.

a)

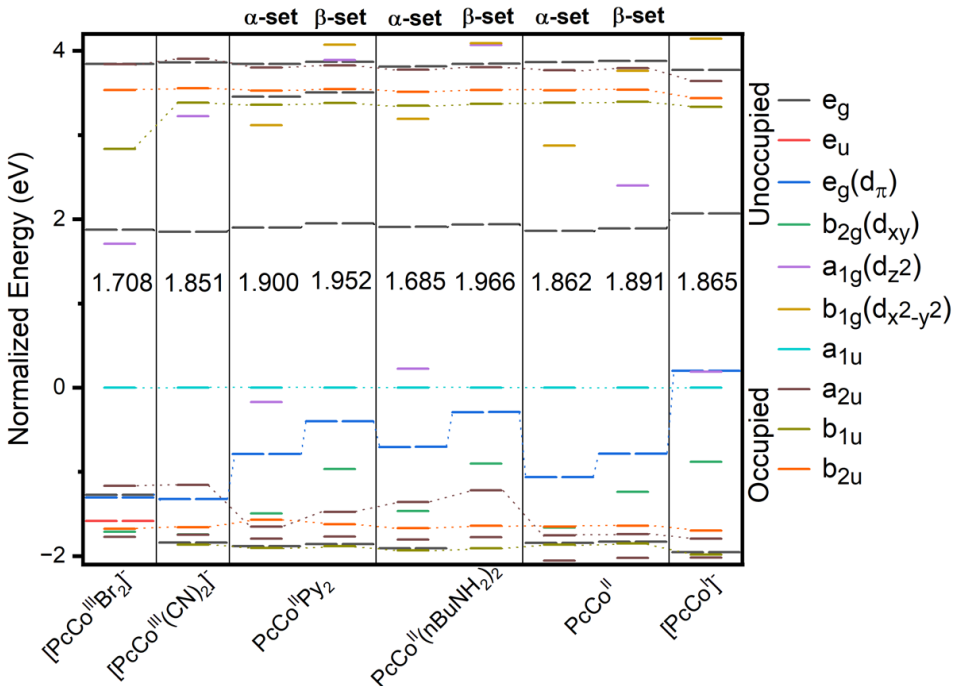
α-set β-set α-set β-set α-set β-set
Normalized Energy (eV)
4
2
0
−2
1.708 1.851 1.900 1.952 1.685 1.966 1.862 1.891 1.865
Unoccupied
Occupied
e_g
e_u
$e_g(d_\pi)$
$b_{2g}(d_{xy})$
$a_{1g}(d_{z^2})$
$b_{1g}(d_{x^2-y^2})$
a_{1u}
a_{2u}
b_{1u}
b_{2u}
$[PcCo^{III}Br_2]^-$
$[PcCo^{III}(CN)_2]^-$
$PcCo^{II}Py_2$
$PcCo^{II}(nBuNH_2)_2$
$PcCo^{II}$
$[PcCo]^-$

b)

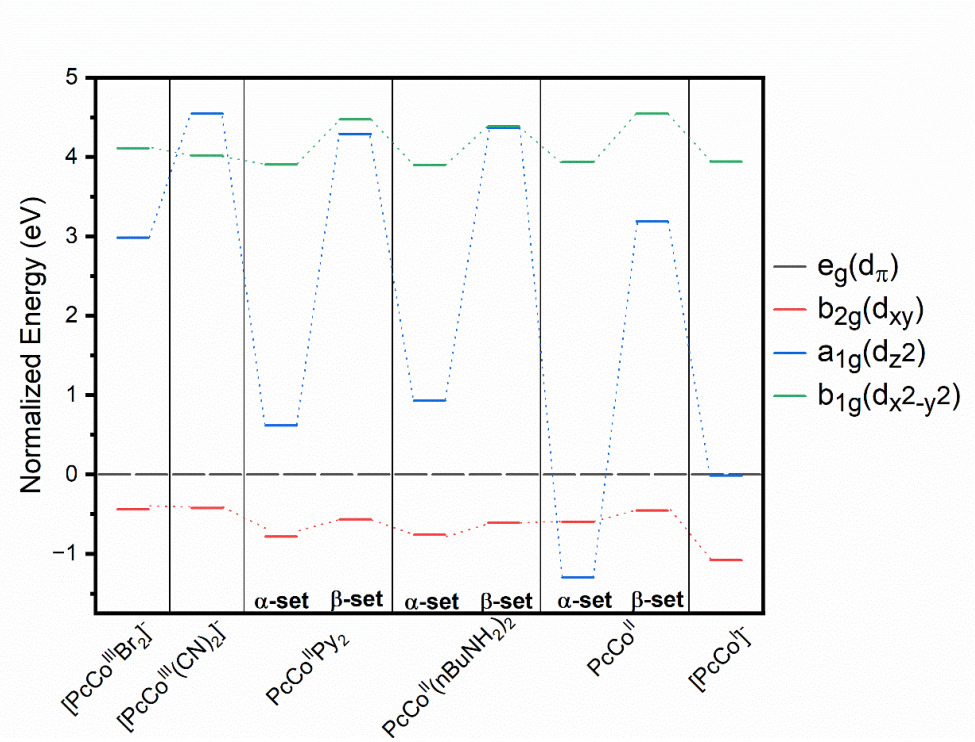
Normalized Energy (eV)
5
4
3
2
1
0
−1
α-set β-set α-set β-set α-set β-set
$e_g(d_\pi)$
$b_{2g}(d_{xy})$
$a_{1g}(d_{z^2})$
$b_{1g}(d_{x^2-y^2})$
$[PcCo^{III}Br_2]^-$
$[PcCo^{III}(CN)_2]^-$
$PcCo^{II}Py_2$
$PcCo^{II}(nBuNH_2)_2$
$PcCo^{II}$
$[PcCo]^-$

Figure 8. DFT-predicted energy diagrams for the frontier orbital manifolds of cobalt phthalocyanine derivatives (relative to the phthalocyanine-centered $1a_{1u}$ MO, a) and zoomed-in d-orbital manifold (relative to the cobalt-centered e_g MOs, b).

Table 3. DFT-predicted molecular orbital compositions for paramagnetic cobalt(II) complexes;[a]

Pc(2-)Co^{II}(*n*$BuNH_2$)$_2$[b]											
		α-set					***β-set***				
MO	E, eV	Symm	Pc	Co	$nBuNH_2$	MO	E, eV	Symm	Pc	Co	*n*$BuNH_2$
198	0.171	a_u	99.93	0.04	0.03	197	-0.136	a_g	5.78	87.82	6.400
197	-0.204	a_g	5.51	87.48	7.01	196	-0.867	a_g	54.54	44.73	0.73
196	*-1.113*	a_g	*99.07*	*0.83*	*0.11*	195	-0.888	a_g	11.87	63.68	24.45
195	*-1.115*	a_g	*98.51*	*1.18*	*0.31*	*194*	*-1.111*	a_g	*98.91*	*0.99*	*0.10*
194	-1.150	a_u	91.04	6.05	2.91	*193*	*-1.113*	a_g	*98.4*	*1.29*	*0.31*
193	-1.415	a_u	99.68	0.04	0.28	192	-1.153	a_u	91.07	6.01	2.93
192	-1.581	a_u	99.8	0.07	0.12	191	-1.424	a_u	99.67	0.04	0.28
191	-1.736	a_g	56.22	43.51	0.26	190	-1.588	a_u	99.8	0.08	0.12
190	*-3.018*	a_g	*95.48*	*4.09*	*0.43*	*189*	*-2.991*	a_g	*93.14*	*6.38*	*0.48*
189	***-3.020***	***a_g***	***95.39***	***4.09***	***0.53***	***188***	***-2.992***	***a_g***	***93.1***	***6.36***	***0.53***
188	***-4.705***	***a_g***	***15.08***	***45.14***	***39.78***	***187***	***-4.958***	***a_u***	***99.94***	***0.01***	***0.05***
187	-4.928	a_u	99.94	0.01	0.05	*186*	*-5.246*	a_g	*29.19*	*69.94*	*0.87*
186	*-5.631*	a_g	*35.2*	*64.08*	*0.72*	*185*	*-5.252*	a_g	*29.33*	*69.73*	*0.94*
185	*-5.636*	a_g	*35.36*	*63.83*	*0.81*	184	-5.860	a_g	33.16	66.82	0.02
184	-6.288	a_u	55.57	2.27	42.16	183	-6.178	a_u	48.81	2.63	48.56

183	-6.394	a_g	55.92	44.05	0.03	182	-6.598	a_u	99.55	0.02	0.43
182	-6.598	a_u	99.56	0.02	0.42	181	-6.734	a_u	96.74	1.41	1.85
181	-6.733	a_u	96.74	1.41	1.86	*180*	*-6.838*	a_g	*99.41*	*0.31*	*0.28*
180	*-6.835*	a_g	*99.73*	*0.18*	*0.09*	*179*	*-6.839*	a_g	*99.59*	*0.29*	*0.12*
179	*-6.835*	a_g	*99.68*	*0.20*	*0.11*	178	6.865	a_u	99.89	0.02	0.09
178	-6.860	a_u	99.89	0.02	0.09	177	-6.950	a_g	78.11	17.12	4.78

Pc(2-)Co^{II}Py$_2$[c]

α-set						***β-set***					
MO	E, eV	Symm	Pc	Co	Py	MO	E, eV	Symm	Pc	Co	Py
202	0.141	*b*	99.99	0.00	0.01	201	-0.062	*a*	4.37	92.37	3.27
201	-0.090	*a*	4.50	91.64	3.86	200	-0.936	*b*	44.84	28.45	26.71
200	-0.979	*a*	3.59	0.00	96.41	199	-0.982	*a*	3.59	0.00	96.41
199	-1.026	*b*	12.57	1.16	86.28	198	-1.079	*b*	18.52	14.1	67.38
197, 198	-1.138	*e*	96.76	0.84	2.40	197	-1.118	*a*	11.71	58.47	29.82
196	-1.178	*b*	91.95	1.51	6.54	195, 196	-1.137	*e*	96.7	0.96	2.34
195	-1.455	*a*	98.22	0.00	1.78	194	-1.181	*b*	91.9	1.45	6.65
193, 194	-1.524	*e*	4.86	0.63	94.51	193	-1.463	*a*	98.2	0.00	1.8
192	-1.622	*a*	98.69	0.60	0.71	191, 192	-1.500	*e*	4.75	0.71	94.54
191	-1.866	*b*	55.46	43.69	0.86	190	-1.628	*a*	98.68	0.59	0.73
189, 190	***-3.081***	***e***	***94.84***	***3.79***	***1.37***	***188, 189***	***-3.056***	*e*	***92.9***	***5.71***	***1.39***
188	***-4.981***	***b***	***99.98***	***0.01***	***0.01***	***187***	***-5.007***	***b***	***99.98***	***0.00***	***0.01***
187	-5.154	*a*	13.07	46.04	40.89	185, 186	-5.407	*e*	30.82	67.77	1.41

185, 186	-5.770	*e*	38.36	60.36	1.27	184	-5.973	*b*	33.29	66.13	0.59
184	-6.475	*b*	59.56	33.87	6.57	183	-6.482	*b*	70.65	0.45	28.91
183	-6.551	*b*	73.39	8.78	17.83	182	-6.630	*a*	97.82	0.00	2.18
182	-6.631	*a*	97.83	0.00	2.17	181	-6.776	*b*	96.43	0.33	3.24
181	-6.776	*b*	95.88	0.67	3.45	179, 180	-6.866	*e*	99.37	0.35	0.29
179, 180	-6.863	*e*	99.54	0.23	0.23	178	-6.890	a_{1u}	99.27	0.11	0.62
178	-6.887	*a*	99.29	0.16	0.55	176, 177	6.992	e_g	76.10	18.67	5.22

Pc(2-)Co^{II}

α-set					***β-set***				
MO	E, eV	Symm	Pc	Co	MO	E, eV	Symm	Pc	Co
156	0.066	a_{1u}	100	0.00	155	-0.029	a_{1g}	8.33	91.67
155	-0.122	a_{1g}	9.16	90.84	153, 154	-1.239	e_g	99.28	0.72
153, 154	-1.240	e_g	99.37	0.63	152	-1.324	a_{2u}	98.23	1.77
152	-1.335	a_{2u}	97.61	2.39	151	-1.358	b_{1g}	55.45	44.55
151	-1.576	b_{2u}	100	0.00	150	-1.584	b_{2u}	100	0.00
150	-1.722	b_{1u}	100	0.00	149	-1.726	b_{1u}	100	0.00
149	-2.232	b_{1g}	56.95	43.05	148	-2.719	a_{1g}	4.10	95.9
147, 148	***-3.243***	***e_g***	***97.03***	***2.97***	***146, 147***	***-3.229***	***e_g***	***95.99***	***4.01***
146	***-5.105***	***a_{1u}***	***100***	***0.00***	***145***	***-5.120***	***a_{1u}***	***100***	***0.00***
144, 145	-6.169	e_g	52.75	47.25	143, 144	-5.905	e_g	40.6	59.4
143	-6.758	b_{2u}	100	0.00	142	-6.357	b_{2g}	44.7	55.3
142	-6.769	b_{2g}	72.55	27.45	141	-6.761	b_{2u}	100	0.00

141	-6.859	a_{2u}	99.99	0.01	140	-6.860	a_{2u}	99.99	0.01
139, 140	-6.949	e_g	99.92	0.08	138, 139	-6.951	e_g	99.9	0.10
138	-6.969	b_{1u}	100	0.00	137	-6.972	b_{1u}	100	0.00
137	-7.161	a_{2u}	98.04	1.96	136	-7.142	a_{2u}	98.45	1.55

[a] Frontier orbitals are formatted in bold. The C^2 method was used to calculate contributions. [b] Effective symmetry of the Pc(2-)Co^{II}(nBuNH_2)$_2$ complex is D_{4h}. However, the highest possible point group in DFT calculations is C_i. Thus, orbital symmetries in this table are provided for C_i point group. [c] Effective symmetry of the Pc(2-)$Co^{II}Py_2$ complex is D_{4h}. However, the highest possible point group in DFT calculations is D_{2d}. Thus, orbital symmetries in this table are provided for the D_{2d} point group.

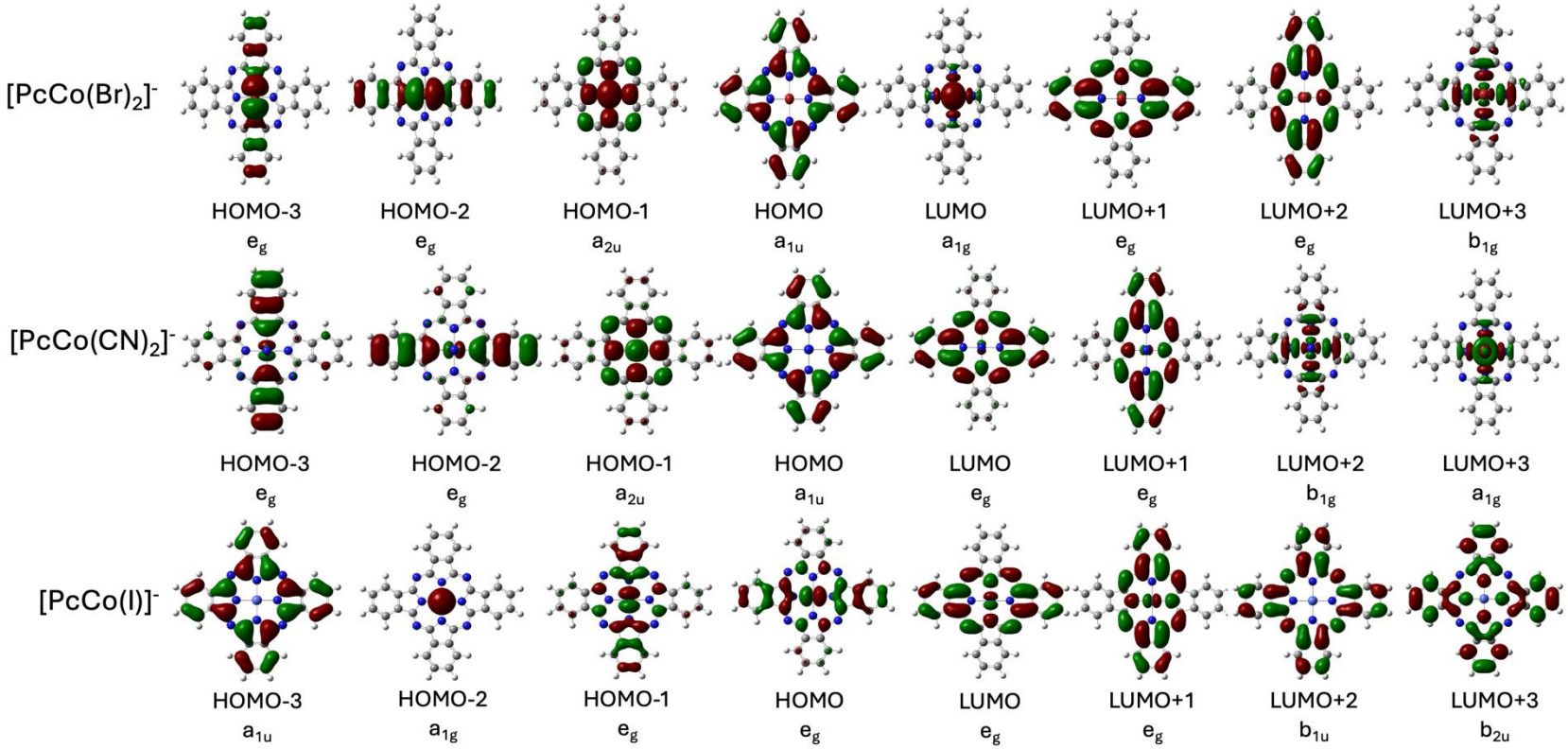

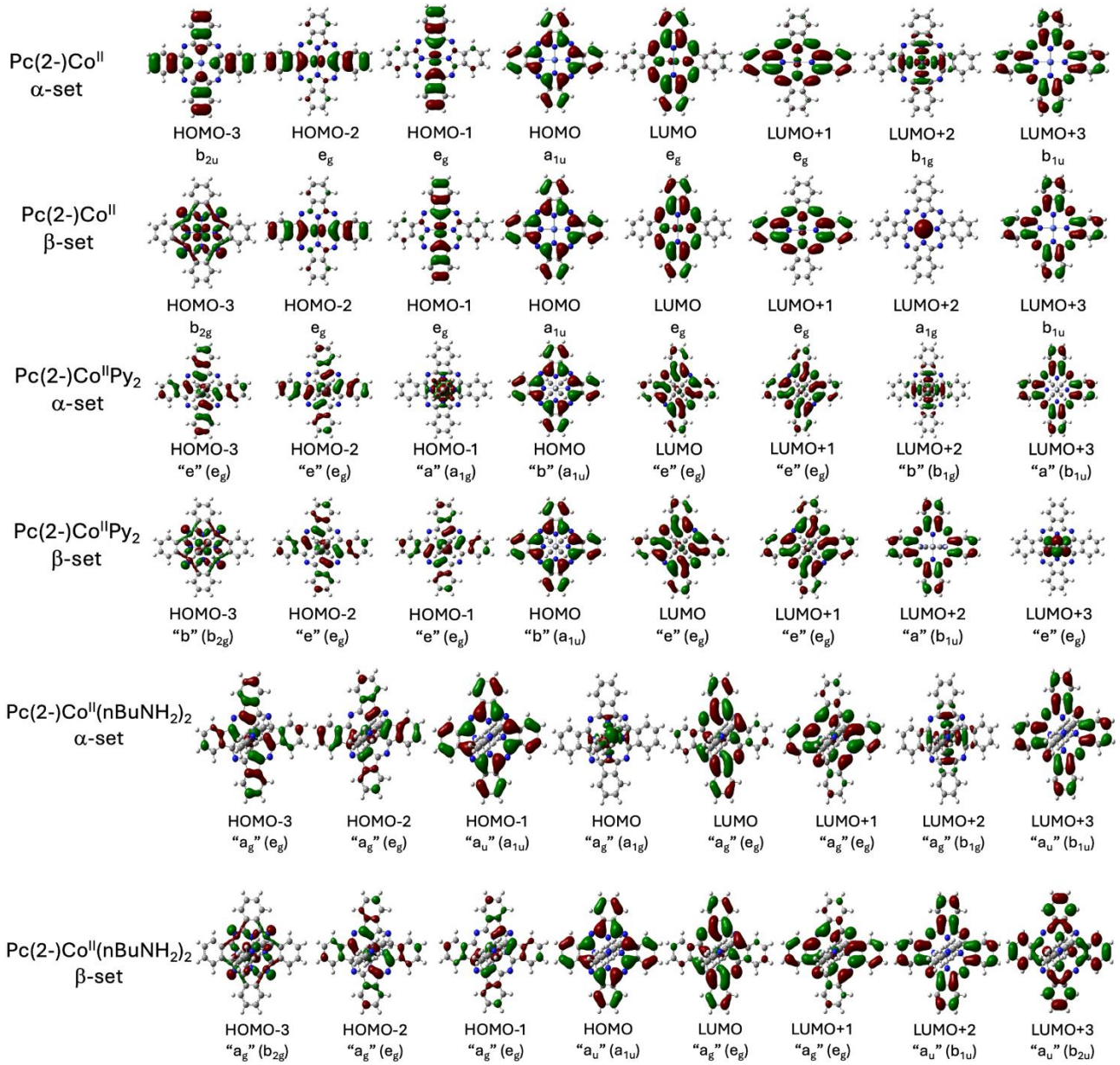
Pc(2-)Co^{II} α-set
HOMO-3 b_{2u}
HOMO-2 e_g
HOMO-1 e_g
HOMO a_{1u}
LUMO e_g
LUMO+1 e_g
LUMO+2 b_{1g}
LUMO+3 b_{1u}
Pc(2-)Co^{II} β-set
HOMO-3 b_{2g}
HOMO-2 e_g
HOMO-1 e_g
HOMO a_{1u}
LUMO e_g
LUMO+1 e_g
LUMO+2 a_{1g}
LUMO+3 b_{1u}
Pc(2-)Co^{II}Py$_2$ α-set
HOMO-3 "e" (e_g)
HOMO-2 "e" (e_g)
HOMO-1 "a" (a_{1g})
HOMO "b" (a_{1u})
LUMO "e" (e_g)
LUMO+1 "e" (e_g)
LUMO+2 "b" (b_{1g})
LUMO+3 "a" (b_{1u})
Pc(2-)Co^{II}Py$_2$ β-set
HOMO-3 "b" (b_{2g})
HOMO-2 "e" (e_g)
HOMO-1 "e" (e_g)
HOMO "b" (a_{1u})
LUMO "e" (e_g)
LUMO+1 "e" (e_g)
LUMO+2 "a" (b_{1u})
LUMO+3 "e" (e_g)
Pc(2-)Co^{II}(nBuNH$_2$)$_2$ α-set
HOMO-3 "a_g" (e_g)
HOMO-2 "a_g" (e_g)
HOMO-1 "a_u" (a_{1u})
HOMO "a_g" (a_{1g})
LUMO "a_g" (e_g)
LUMO+1 "a_g" (e_g)
LUMO+2 "a_g" (b_{1g})
LUMO+3 "a_u" (b_{1u})
Pc(2-)Co^{II}(nBuNH$_2$)$_2$ β-set
HOMO-3 "a_g" (b_{2g})
HOMO-2 "a_g" (e_g)
HOMO-1 "a_g" (e_g)
HOMO "a_u" (a_{1u})
LUMO "a_g" (e_g)
LUMO+1 "a_g" (e_g)
LUMO+2 "a_u" (b_{1u})
LUMO+3 "a_u" (b_{2u})

Figure 9. DFT-predicted frontier orbitals in cobalt phthalocyanines; the isosurface value of the orbitals is 0.02. For Pc(2-)$Co^{II}Py_2$ and Pc(2-)$Co^{II}(n\text{BuNH}_2)_2$ complexes, the effective D_{4h} symmetries are given in parentheses.

Since modern theoretical methods allow us to calculate the energies of both charge-transfer and π–π* transitions in transition-metal phthalocyanines and their derivatives with high (0.1-0.2 eV) accuracy,[129] it is logical to compare theoretical and experimental (magneto)optical properties of the cobalt phthalocyanine complexes spanning the +1 and +3 oxidation states at the central metal ion and resolve existing controversies. The DFT-predicted energy diagram and frontier MOs for all the target complexes are shown in **Figures 8** and **9** and Supporting Information Figures S6-S11. The DFT-predicted orbital compositions are listed in **Tables 2** and **3**. As expected, the diamagnetic Co(III) derivatives have $(d_{xy})^2(d_{xz,yz})^4$ electronic configurations ($^1A_{1g}$ ground state in D_{4h} symmetry), the paramagnetic (s = ½) Co(II) complexes have $(d_{xy})^2(d_{xz,yz})^4(d_{z2})^1$ electronic configurations ($^2A_{1g}$ ground state in D_{4h} effective symmetry), and the diamagnetic cobalt(I) anion has a $(d_{xy})^2(d_{xz,yz})^4(d_{z2})^2$ electronic configuration ($^1A_{1g}$ ground state in D_{4h} symmetry). The DFT-predicted presence of the unpaired electron in the d_{z2} orbital in cobalt(II) derivatives correlates well with the EPR spectra of these complexes. The corresponding DFT-predicted spin densities are shown in Supporting Information Figure S12. The transitions allowed by group theory for these states are listed in **Tables 4-6** and graphically shown in **Figures 10-12**.

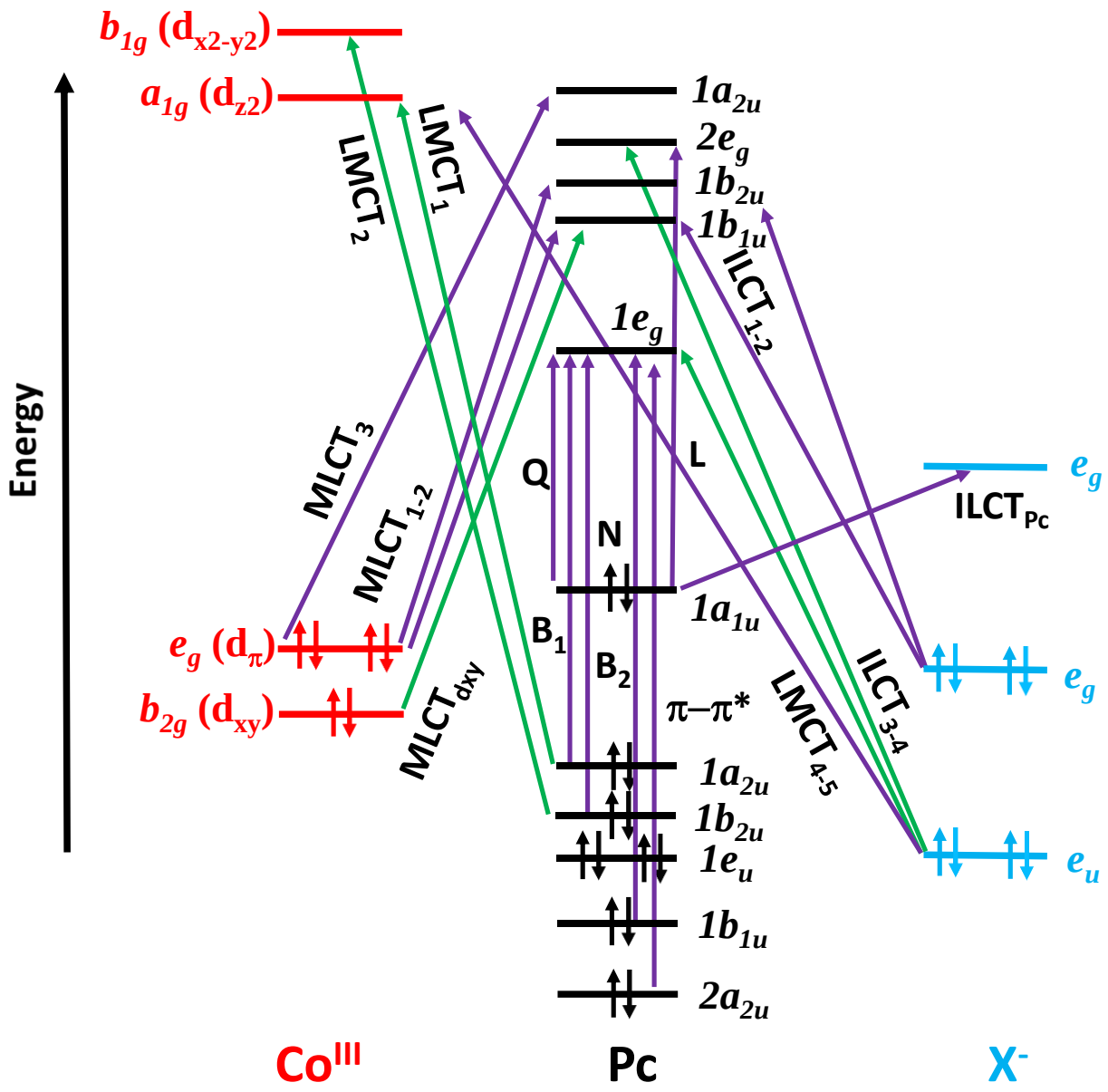

Figure 10. Simplified diagram for symmetry-allowed transitions in cobalt(III) phthalocyanines with D_{4h} symmetry. Magenta arrows show transitions that should result in degenerate excited states and MCD *A*-terms.

Table 4. Allowed charge-transfer transitions for low-spin (S = 0) cobalt(III) phthalocyanines.[a]

Single-electron transition	Excited state	CT type	Polarization	Expected MCD term
$e_g \rightarrow b_{1u}^*, b_{2u}^*, a_{2u}^*, a_{1u}^*$	^1E_u	MLCT or ILCT	x,y	*A*
$b_{2g} \rightarrow b_{1u}^*$	$^1A_{2u}$	MLCT	z	*B*
$b_{2u} \rightarrow b_{1g}^*$	$^1A_{2u}$	LMCT	z	*B*
$a_{2u} \rightarrow a_{1g}^*$	$^1A_{2u}$	LMCT	z	*B*
$e_u \rightarrow b_{1g}^*, a_{1g}^*$	^1E_u	LMCT	x,y	*A*
$e_u \rightarrow e_g^*$	$^1A_{2u}$	ILCT	z	*B*

[a] The ground-state configuration of cobalt(III) is $(b_{2g})^2(e_g)^4$ and the ground state symmetry term is $^1A_{1g}$.

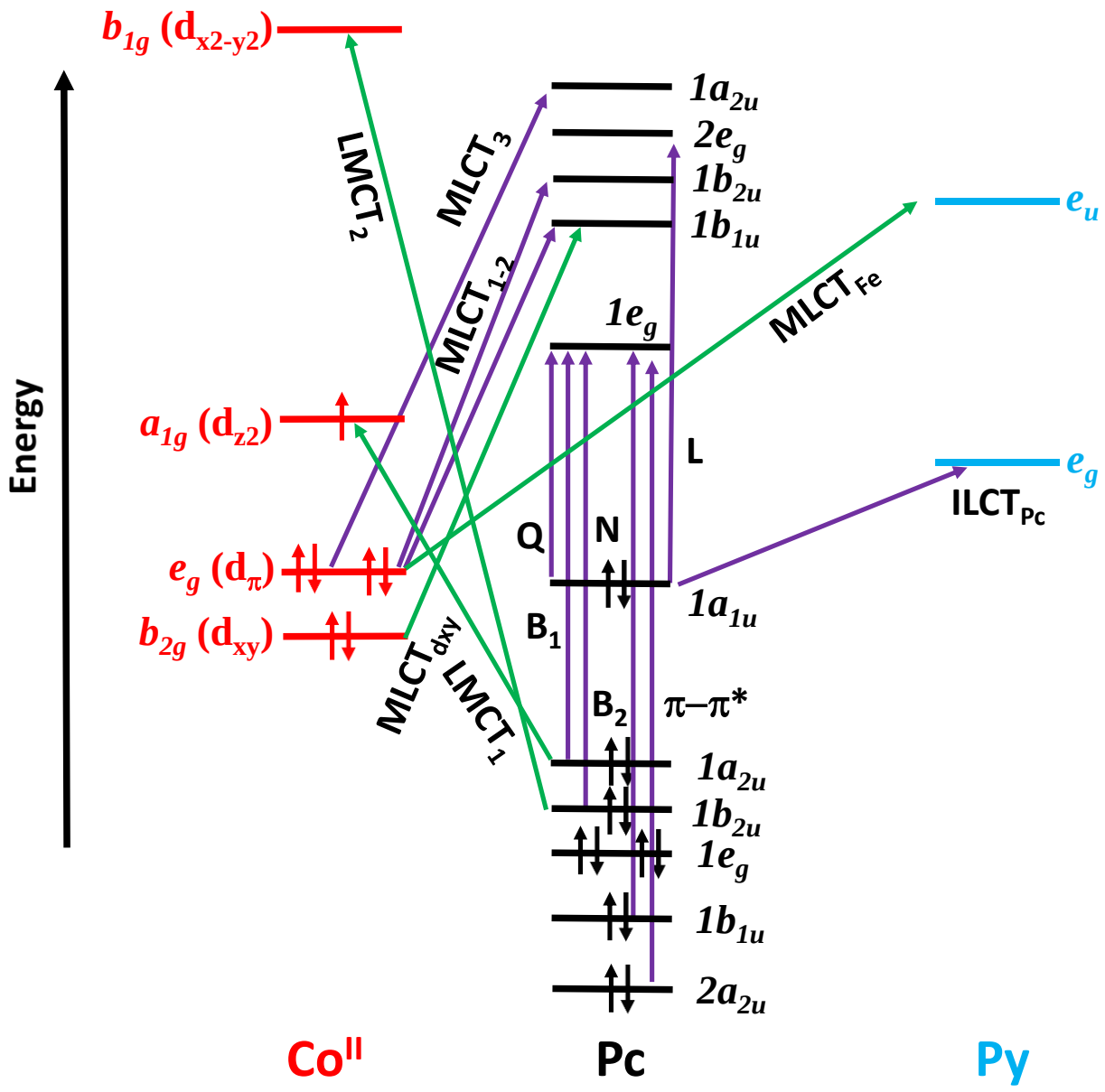

Figure 11. Simplified diagram for symmetry-allowed transitions in cobalt(II) phthalocyanines with D_{4h} (effective) symmetry. Magenta arrows show transitions that should result in degenerate excited states and MCD *A*-terms.

Table 5. Allowed charge-transfer transitions for low-spin (S = 1/2) cobalt(II) phthalocyanines.[a]

Single-electron transition	Excited state	CT type	Polarization	Expected MCD term
$e_g \rightarrow b_{1u}^*, b_{2u}^*, a_{2u}^*, a_{1u}^*$	^1E_u	MLCT	x,y	*A*
$b_{2g} \rightarrow b_{1u}^*$	$^1A_{2u}$	MLCT	z	*B*
$a_{1g} \rightarrow a_{2u}^*$	$^1A_{2u}$	MLCT	z	*B*
$e_g \rightarrow e_u^*$	$^1A_{2u}$	MLCT	z	*B*
$b_{2u} \rightarrow b_{1g}^*$	$^1A_{2u}$	LMCT	z	*B*
$a_{2u} \rightarrow a_{1g}^*$	$^1A_{2u}$	LMCT	z	*B*
$b_{1u}, b_{2u}, a_{2u}, a_{1u} \rightarrow e_g^*$	^1E_u	ILCT	x,y	*A*

[a] The ground-state configuration of cobalt(III) is $(b_{2g})^2(e_g)^4(d_{z2})^1$ and the ground state symmetry term is $^2A_{1g}$.

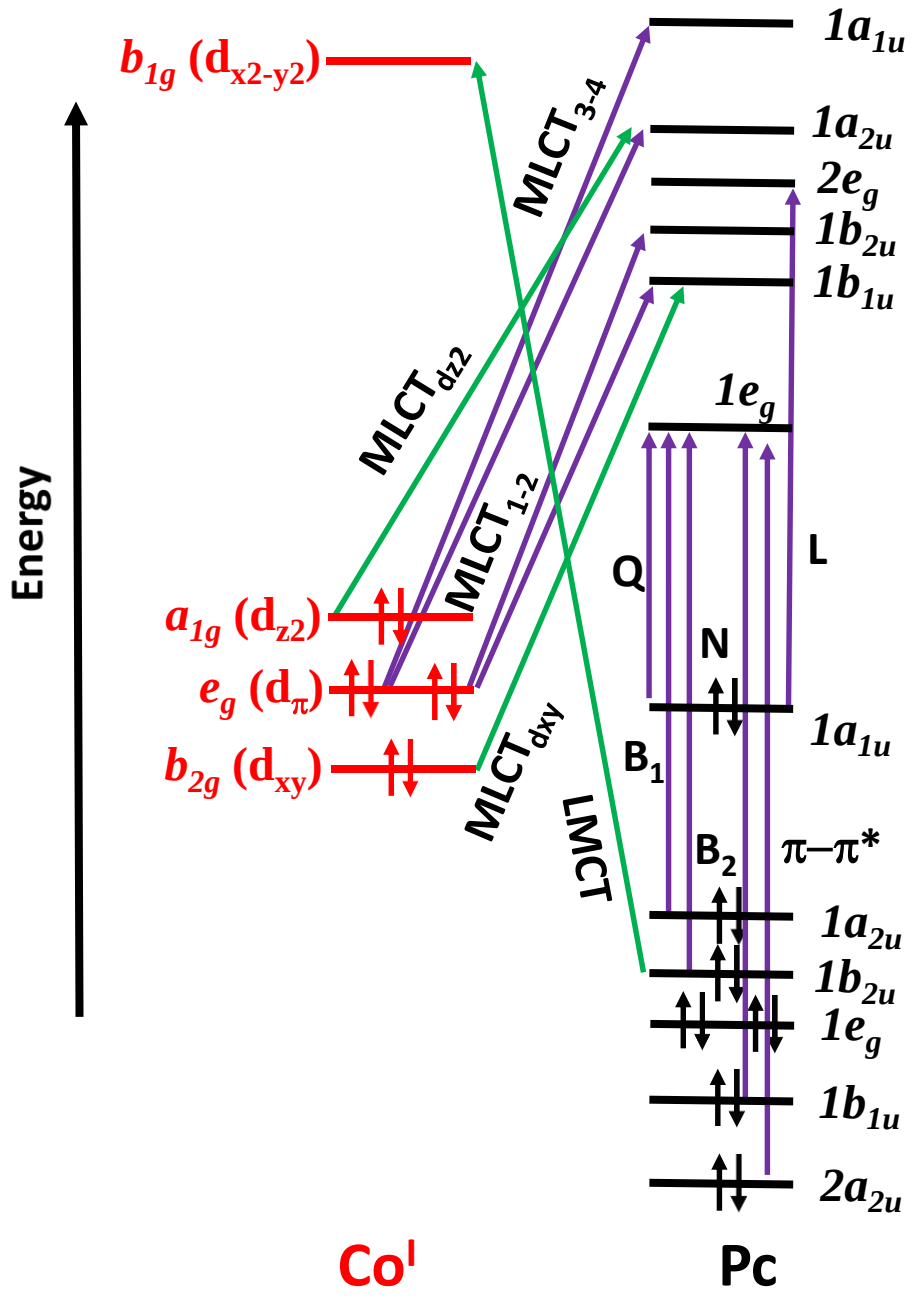

Figure 12. Simplified diagram for symmetry-allowed transitions in cobalt(I) phthalocyanines with D_{4h} symmetry. Magenta arrows show transitions that should result in degenerate excited states and MCD *A*-terms.

Table 6. Allowed charge-transfer transitions for low-spin (S = 0) cobalt(I) phthalocyanines.[a]

Single-electron transition	Excited state	CT type	Polarization	Expected MCD term
$e_g \rightarrow b_{1u}^*, b_{2u}^*, a_{2u}^*, a_{1u}^*$	^1E_u	MLCT	x,y	*A*
$b_{2g} \rightarrow b_{1u}^*$	$^1A_{2u}$	MLCT	z	*B*
$a_{1g} \rightarrow a_{2u}^*$	$^1A_{2u}$	MLCT	z	*B*
$b_{2u} \rightarrow b_{1g}^*$	$^1A_{2u}$	LMCT	z	*B*

[a] The ground-state configuration of cobalt(III) is $(b_{2g})^2(e_g)^4(d_{z2})^2$ and the ground state symmetry term is $^1A_{1g}$.

In the case of $[Pc(2-)Co^{III}Br_2]^-$, one might expect that the long Co-Br bond distance and weak axial ligand field result in a relatively stable unoccupied d_{z2} orbital and bromide contribution to the occupied frontier orbitals. Indeed, DFT calculations predict that the LUMO in this complex has nearly equal contributions from the cobalt(III) d_{z2} orbital and two bromine ligands (**Table 2**). Additionally, bromide contributes to the HOMO-2/-3 (e_g (Br)) pair of MOs and the HOMO-6/-7 (e_u (Br)) pair of MOs. Cobalt-centered d_π orbitals form the HOMO-4/-5 (e_g (d_π)) pair and are well-separated (~1.3 eV) from the phthalocyanine-centered HOMO ($1a_{1u}$). This situation is very different from $Pc(2-)Fe^{II}L_2$ derivatives with the same d^6 electron configuration and spin state in which iron-centered orbitals are close in energy to the phthalocyanine-centered $1a_{1u}$ orbital.[112,130] This difference can be explained by the change in oxidation state in cobalt(III) *versus* iron(II). Unsurprisingly, such stabilization leads to significantly higher TDDFT-predicted energies of

MLCT1 (e_g (d_π) → $1b_{1u}$*) and MLCT2 (e_g (d_π) → $1b_{2u}$*) compared to the iron(II) analogs.[112] Indeed, these charge-transfer bands were predicted at 281 and 269 nm, respectively (**Table S1**). Since MLCT1 and MLCT2 transitions are located in the B-band region, they heavily overlap with a number of the other bands, making their identification in the experimental spectra nearly impossible. Since the LUMO has predominantly Co/Br character and the HOMO and HOMO-1 are predominantly phthalocyanine-centered orbitals, it opens the possibility for Pc → LUMO symmetry forbidden LMCT1 ($1a_{1u}$ → a_{1g}* (Co d_{z2}/Br)) and symmetry allowed LMCT2 ($1a_{2u}$ → a_{1g}* (Co d_{z2}/Br)) transitions. Indeed, the symmetry-allowed LMCT2 band was predicted by TDDFT calculations at 477 nm and can be associated with the MCD *B*-term observed at 440 nm (**Figure 13 and Table S1**). Additionally, TDDFT calculations predict two closely spaced doubly degenerate transitions at 445 and 434 nm that have fairly strong intensities. These are heavily dominated by $1e_u$ (Br) → a_{1g}* (Co d_{z2}/Br) and $1a_{2u}$ (Pc) → $1e_g$* (Pc) single-electron excitations, with the former contribution accounting slightly more for the first excited state and the latter contribution accounting slightly more for the second excited state **(Table S1**). These could be responsible for the MCD *A*-term (B1 band) observed at 408 nm in the spectrum of [Pc^{tBu}(2-)$Co^{III}Br_2$]$^-$ (**Figure 13**). We are unsure of the nature of the 511 nm band observed in the absorption spectrum of this compound. This band has no intensity in the MCD spectrum in a 1.6 T magnetic field, while TDDFT calculations predict two symmetry-forbidden excited states in this region. The first one predicted at 509 nm originates from an almost pure $1a_{1u}$ → b_{1g}* (Co d_{x2-y2}/Pc) single-electron transition and has substantial LMCT character. The second state is doubly degenerate and originates from e_g (Br) → a_{1g}* (Co d_{z2}/Br) (93%) single-electron excitations (predicted at 486 nm). Homberg and co-authors have shown that the ~510 nm band in [Pc(2-)$Co^{III}Br_2$]$^-$ undergoes a systematic blue shift when axial bromide ligands are replaced with chloride and fluoride ligands.[71]

Since the influence of the axial ligands on the energies of the $1a_{1u}$ (Pc) and b_{1g}* (Co d_{x2-y2}/Pc) orbitals is expected to be small, while the energies of the e_g (Br) and a_{1g}* (Co d_{z2}/Br) orbitals should strongly depend on the nature of the axial ligands, we can speculate that the 511 nm band is dominated by the e_g (Br) → a_{1g}* (Co d_{z2}/Br) single-electron excitation, which gains intensity *via* vibronic coupling. Next, two more symmetry-allowed non-degenerate charge-transfer bands were predicted around 390 nm. One band is dominated (92%) by the e_u (Br) → $1e_g$* (Pc) single-electron excitation, and the other has 93% of $2a_{2u}$ (Pc) → a_{1g}* (Co d_{z2}/Br) LMCT nature. Phthalocyanine-centered (here and below, we are following Stillman's nomenclature for the phthalocyanine-centered excited states)[131] Q- ($1a_{1u}$ → $1e_g$*), B2- ($1b_{2u}$ → $1e_g$*), $2a_{2u}$ → $1e_g$*, B3- ($1b_{1u}$ → $1e_g$*) and L-bands ($1a_{1u}$ → $2e_g$*) were predicted at 662, 374, 356, 349, and 340 nm and are closely related to the bands observed in the UV-Vis and MCD spectra of $[Pc^{tBu}(2\text{-})Co^{III}Br_2]^-$ (**Figure 13**). Finally, two more symmetry-allowed doubly degenerate charge-transfer transitions were predicted by TDDFT calculations between 300 and 330 nm (Table S1). The first one (329 nm) belongs to almost pure $1e_u$ (Pc) → a_{1g}* (Co d_{z2}/Br) single-electron excitation, while the second (316 nm) has e_u (Br) → b_{1g}* (Co d_{x2-y2}/Pc) single-electron excitation character.

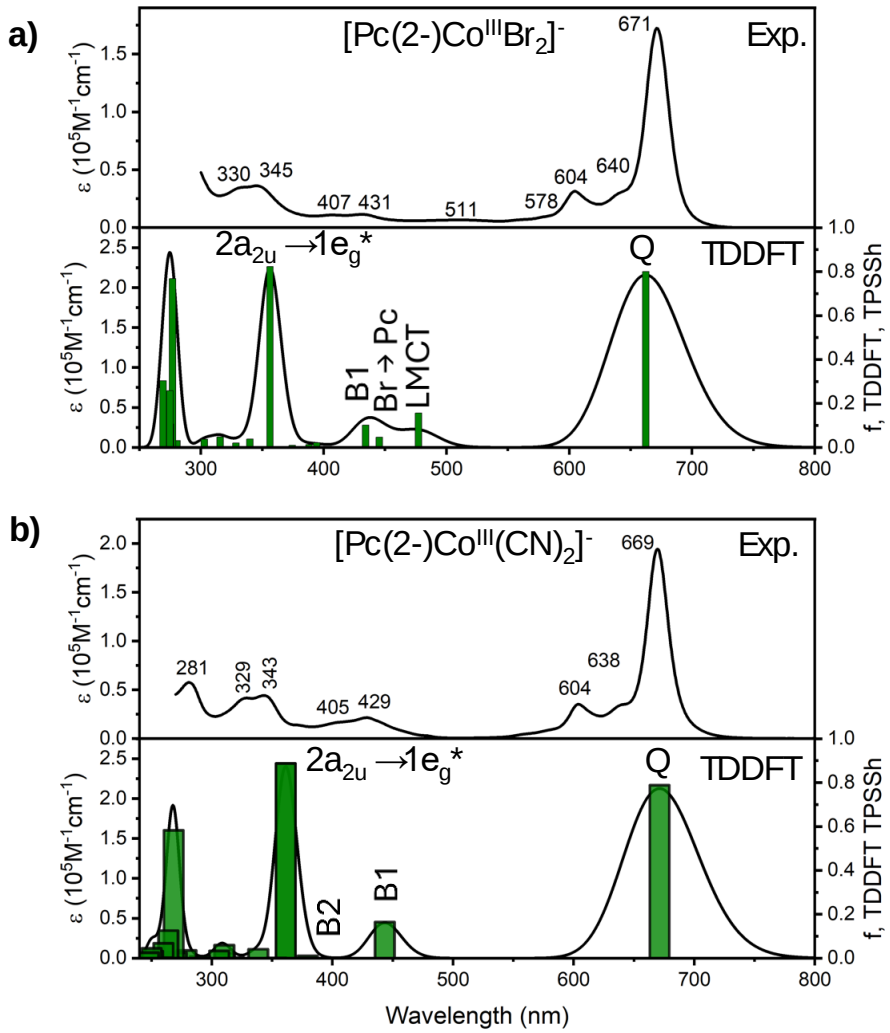

Figure 13. Experimental (top) *versus* TDDFT-predicted (bottom) UV-Vis spectra of [Pc(2-)$Co^{III}Br_2]^-$ (a) and [Pc(2-)$Co^{III}(CN)_2]^-$ (b).

In the case of the [Pc(2-)$Co^{III}(CN)_2]^-$ anion, one might expect that because of the shorter Co-CN bond distance and strong axial ligand field, the unoccupied d_{z2} orbital will be destabilized relative to the phthalocyanine-centered *1e*$_g$* orbitals. Indeed, DFT calculations predict that the LUMO and LUMO+1 in this complex are the classic Gouterman *1e*$_g$* orbitals[132-134] followed by

the d_{x2-y2} (45%)/Pc (55%) LUMO+2 and d_{z2} (41%)/CN (35%)/Pc (24%) LUMO+3 (Table 2). These orbitals are predicted to have ~0.9 and ~1.4 eV higher energies than the Gouterman $1e_g$* MOs. In addition, the cyanide ligands contribute to the HOMO-1 ($1a_{2u}$ orbital), although their contribution to this orbital is smaller than that of the bromide ligands in [Pc(2-)$Co^{III}Br_2$]$^-$. The energy separation between phthalocyanine-centered $1a_{1u}$ HOMO and $1a_{2u}$ HOMO-2 is similar for both complexes. Finally, the axial ligands contribute to the HOMO-10/-11 (e_g (CN/d_π)) pair of MOs and the HOMO-15/-16 (e_u (CN/Pc)) pair of MOs. Cobalt-centered d_π orbitals form the HOMO-2/-3 (e_g (d_π)) pair, which is, again, ~1.3 eV more stable than the phthalocyanine-centered HOMO. Such electronic structure precludes observation of the low-energy LMCT and MLCT transitions. Indeed, energies of the MLCT1 (e_g (d_π) → $1b_{1u}$*) and MLCT2 (e_g (d_π) → $1b_{2u}$*) transitions were predicted at 279 and 268 nm, respectively, which is very close to the energies predicted for [Pc(2-)$Co^{III}Br_2$]$^-$ (**Table S1**). TDDFT-predicted LMCT transitions can be separated into two groups. The first group consists of the non-degenerate transitions. These are dominated by the $1b_{2u}$ → b_{1g}* (d_{x2-y2}), $1a_{2u}$ → a_{1g}* (d_{z2}), and $2a_{2u}$ → a_{1g}* (d_{z2}) single-electron excitations predicted at 311, 310, and 264 nm (**Table S1**) and should result in MCD *B*-terms. The second group consists of two degenerate excited states that are dominated by the $1e_u$ → b_{1g}* (d_{x2-y2}) and $2e_u$ (CN/Pc) → b_{1g}* (d_{x2-y2}) single-electron excitations predicted at 264 and 250 nm. These excited states should be associated with MCD *A*-terms and are LMCT in nature. Only one symmetry-forbidden LMCT band was predicted between phthalocyanine-centered Q- and B1-bands. It has pure $1a_{1u}$ → b_{1g}* (d_{x2-y2}) nature and was predicted at 541 nm. The following phthalocyanine-centered degenerate excited states were predicted by TDDFT calculations: Q- ($1a_{1u}$ → $1e_g$*, 671 nm), B1- ($1a_{2u}$ → $1e_g$*, 443 nm), B2- ($1b_{2u}$ → $1e_g$*, 379 nm), $2a_{2u}$ → $1e_g$* (361 nm), B3- ($1b_{1u}$ → $1e_g$*, 354 nm), L-bands ($1a_{1u}$ → $2e_g$*, 339 nm), $2a_{1u}$ → $1e_g$* (306 nm), $3a_{2u}$ → $1e_g$* (271 nm), and $1a_{2u}$ → $2e_g$* (260

nm). Thus, it seems that the 390 - 500 nm spectral region should only have the B1 band (which is unlikely judging from the MCD spectrum of $[Pc(2-)Co^{III}(CN)_2]^-$), while the other π–π^* transitions should be located between 250 and 390 nm. Considering typical TDDFT calculation errors (0.1-0.2 eV), we speculate that the B2-band can also contribute to this spectral envelope.

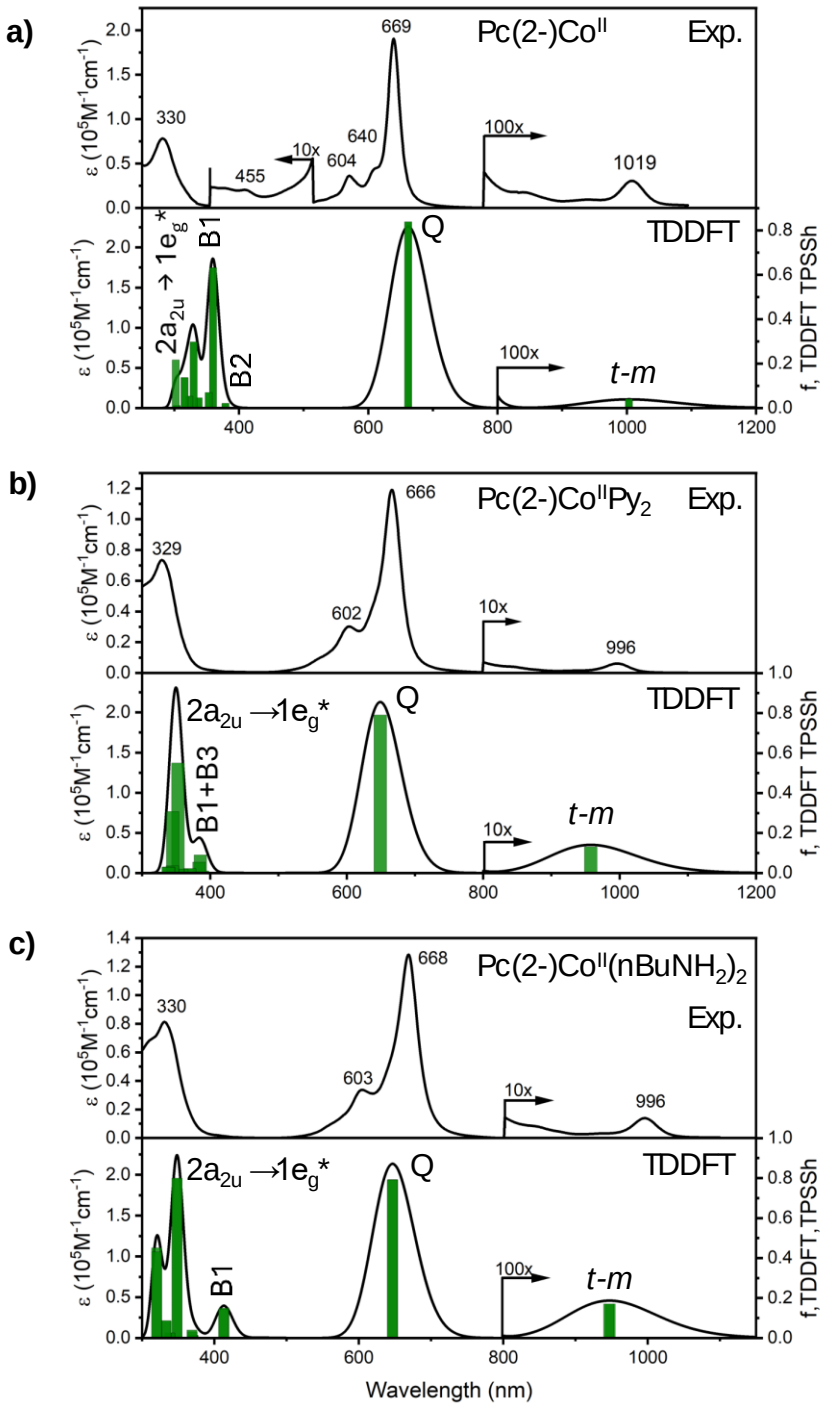

Figure 14. Experimental (top) *versus* TDDFT-predicted (bottom) UV-Vis spectra of Pc(2-)Co^{II} (a), Pc(2-)$Co^{II}Py_2$ (b), and Pc(2-)$Co^{II}(n BuNH_2)_2$ (c).

For Pc(2-)Co^{II}, one might expect that the energies of the d_π orbitals will be between those predicted for cobalt(III) and cobalt(I) species. Indeed, DFT predicts that the HOMO in Pc(2-)Co^{II} has $1a_{1u}$ symmetry, and the HOMO-1 and HOMO-2 are cobalt d_π orbitals (**Table 3**). Cobalt-centered d_π orbitals are ~0.9 eV more stable than the phthalocyanine-centered HOMO. In addition, the unoccupied d_{x2-y2} orbital is ~1.4 eV higher in energy compared to the d_{z2} orbital (β-set). The LUMO and LUMO+1 in this complex are classic Gouterman $1e_g$* orbitals.[132-134] The lowest energy symmetry allowed LMCT transition should originate from the $1a_{2u} \rightarrow a_{1g}$ (d_{z2}) single-electron excitation. The $1a_{1u}$-$1a_{2u}$ energy gap (β-set) is ~1.7 eV and the $1e_g^* \rightarrow d_{z2}^*$ energy separation is ~0.5 eV. Such electronic structure precludes observation of the low-energy LMCT and MLCT transitions. Indeed, the energies of the MLCT1 (e_g (d_π) → $1b_{1u}$*) and MLCT2 (e_g (d_π) → $1b_{2u}$*) transitions were predicted at 323 and 316 nm, respectively, while the LMCT transition was predicted at 329 nm (**Table S2**). These should be observed in the B-band region. TDDFT calculations predict phthalocyanine-centered degenerate excited states at 662 nm (Q-band, $1a_{1u} \rightarrow 1e_g$*), 379 nm (B2-band, $1b_{2u} \rightarrow 1e_g$*), 360 nm (B1-band, $1a_{2u} \rightarrow 1e_g$*), 353 nm (B3-band, $1b_{1u} \rightarrow 1e_g$*), 338 nm (L-band $1a_{1u} \rightarrow 2e_g$*), and 330 nm (π–π*, $2a_{2u} \rightarrow 1e_g$*). Again, except for the Q-band, all of these bands should be observed in the B-band region. Additionally, the mixed π–π*/MLCT (56% of $2a_{1u} \rightarrow 1e_g$* and 25% $d_\pi \rightarrow 1b_{1u}$*) band was predicted at 302 nm. TDDFT also correctly predicts the presence of a *t-m* transition in the NIR region of the Pc(2-)Co^{II} complex (predicted at 1003 nm, **Table S2**). The presence of such transitions in the experimental NIR spectra of the open-shell transition-metal phthalocyanines was pointed out by Lever and co-workers,[90] while theoretical aspects for such excitations were provided by Zerner and Cory.[91] In short, the metal-ligand exchange coupling in paramagnetic transition-metal phthalocyanines should result in a non-zero intensity to the *t-m* transitions and should give rise to the Q-band-like absorption that

originates from the spin-forbidden $1a_{1u}$ (^{1}Pc) → $1e_g$* (^{3}Pc) single-electron excitation that brings the phthalocyanine chromophore from a singlet to a triplet state (**Figure 2**). Considering that the single-electron excitations in the $1a_{1u}$ (^{1}Pc) → $1e_g$* (^{1}Pc) (Q-band) and the $1a_{1u}$ (^{1}Pc) → $1e_g$* (^{3}Pc) (*t-m* transition) are the same, we expect that the observed *t-m* transition will have a vibronic profile close to that observed for a regular Q-band. By analogy, the MCD spectra of the *t-m* band should resemble (at least for 0-0 transitions) the MCD signature of the spin-allowed Q-band. Next, since ligand-metal exchange integrals K_{im} and K_{am} should be small, the energies of the $^4\Psi_{II}$ and $^2\Psi_{II}$ states are expected to be close to each other (**Figure 2**), leading to contamination of the doublet state by the quartet state. Indeed, TDDFT-predicted $<S^2>$ values for the *t-m* transitions in PcCo^{II} are significantly higher than those expected for the transitions in a simple s = 1/2 system (**Table S2**). TDDFT calculations also correctly predict a greatly decreased oscillator strength for the *t-m* transition compared to the Q_{0-0} band. Overall, TDDFT predictions for the Pc(2-)Co^{II} complex are in good agreement with the experimental data and indicate the presence of the NIR *t-m* transitions, Q-bands, number of the excited states in the B-band region, and the window between 400 and 550 nm.

Although the effective symmetry of the Pc(2-)Co^{II}Py$_2$ complexes is D_{4h}, the highest symmetry that can be used in the DFT calculations of this compound is D_{2d} (for obvious reasons). Elimination of the inversion center in DFT geometry leads to heavier mixing of the excited state expansion vectors and allows some transitions forbidden under D_{4h} point group restrictions. Adding axial pyridine ligands to Pc(2-)Co^{II} has several consequences for its electronic structure. First, the axial coordination significantly destabilizes the energy of the d_{z2} orbital relative to the Gouterman[132-134] LUMO/LUMO+1 pair ($\Delta 1e_g$*-d_{z2} is ~0.5 eV in Pc(2-)Co^{II} and ~1.9 eV in Pc(2-)Co^{II}Py$_2$, respectively; we will keep D_{4h} point group notation in the discussion part, while actual

D_{2d} point group notation for Pc(2-)$Co^{II}Py_2$ in **Tables 3** and **8**), while the energy gap between the phthalocyanine-centered $1a_{1u}$ HOMO and d_π orbitals gets smaller (~0.8-1.0 eV for Pc(2-)Co^{II} versus ~0.4-0.8 eV for Pc(2-)$Co^{II}Py_2$). Third, a pair of degenerate, unoccupied, pyridine-centered orbitals were predicted at ~1.5 eV above the Gouterman LUMO/LUMO+1 $1e_g$* pair. Pyridine ligand lone pairs also mix with the cobalt d_{z2} orbital. Thus, pyridine coordination adds metal-to-axial ligand and phthalocyanine-to-axial ligand charge transfer transitions to the overall picture (**Figure 11** and **Table S2**). Indeed, several such transitions were predicted by the TDDFT calculations although their intensities remain low. Out of the two most intense, one is dominated by the $1a_{1u}$ (Pc) → e_g* (Py) single-electron excitation (f = 0.0542, 384 nm) and should result in a MCD *A*-term, while the other one originates from the d_π(Co) → e_g* (Py) single-electron excitation (**f** = 0.0196, 352 nm) and should lead to a MCD *B*-term (this transition is forbidden in D_{4h} but allowed in D_{2d} point group). The *t-m* transition in Pc(2-)$Co^{II}Py_2$ was predicted at 958 nm and correlates well with the experimental data. TDDFT calculations predicted the phthalocyanine-centered degenerate excited states at 649 nm (Q-band, $1a_{1u}$ → $1e_g$*), 385 nm (B1+B3-band, 35% of $1a_{2u}$ → $1e_g$* and 28% of $1b_{1u}$ → $1e_g$*), 370 nm (B2-band, $1b_{2u}$ → $1e_g$*), 353 nm (π–π*, $2a_{2u}$ → $1e_g$*), 345 nm (B3-band, $1b_{1u}$ → $1e_g$*), 339 nm (π–π*, $2a_{1u}$ → $1e_g$*), and 338 nm (L-band $1a_{1u}$ → $2e_g$*). In addition, the MLCT1 (d_π → $1b_{1u}$*) and MLCT2 (d_π → $1b_{2u}$*) bands were predicted at 358 and 345 nm. Again, TDDFT calculations correctly predict the window between Q- and B-band regions.

Lowering the point group symmetry in Pc(2-)Co^{II}(nBuNH_2)$_2$ to C_i results in the complete removal of degeneracy in the DFT orbitals, which complicated the analysis of the DFT and TDDFT results. Nevertheless, we can still recognize and assign the major transitions in this compound predicted by TDDFT. In general, the electronic structure of the Pc(2-)Co^{II}(nBuNH_2)$_2$

complex resembles that of Pc(2-)$Co^{II}Py_2$. Since butylamine is a stronger σ-donor compared to pyridine, it is not surprising to see a further destabilization of the unoccupied (β-set) cobalt-centered d_{z2} orbital relative to the Gouterman[132-134] $1e_g$* pair (~2.1 eV in Pc(2-)Co^{II}(*n*$BuNH_2)_2$ versus ~1.5 eV in Pc(2-)$Co^{II}Py_2$). No predominantly axial ligand-centered unoccupied orbitals are expected close to the frontier orbital energy envelope. However, nitrogen lone pairs from the axial ligands contribute significantly to the phthalocyanine-centered $1a_{2u}$ and cobalt d_{z2} orbitals (**Table 3**). The degenerate *t-m* transition in Pc(2-)Co^{II}(n$BuNH_2)_2$ was predicted at ~947 nm and correlates well with the experimental data, in particular the MCD *A*-term. TDDFT calculations predicted the phthalocyanine-centered nearly degenerate excited states at ~647 nm (Q-band, $1a_{1u} \rightarrow 1e_g$*), ~414 nm (B1-band, $1a_{2u} \rightarrow 1e_g$*), ~349 nm (π–π*, $2a_{2u} \rightarrow 1e_g$*), and ~339 nm (B3-band, $1b_{1u} \rightarrow 1e_g$*). The B2-band is heavily mixed with MLCT components, which were predicted at 371 and 369 nm (**Table S2**). In addition, the almost pure MLCT1 ($d_\pi \rightarrow 1b_{1u}$*) and MLCT2 ($d_\pi \rightarrow 1b_{2u}$*) bands were predicted at 333 and 321 nm. Similar to the other cobalt(II) complexes, TDDFT calculations predict a spectral window between Q- and B-band regions.

Table 7. MCD band centers for Q-band and *t-m* band spectral envelopes from band deconvolution analysis of the UV-Vis-NIR and MCD spectra of $Pc^{tBu}Co$ in toluene.

Q-band region		*t-m* band region	
E, cm^{-1}	λ, nm	E, cm^{-1}	λ, nm
14949[a]	669	10039[a]	996
15100	662	10437	958
15500	645	10650	939
15739	635	10932	915
16086	622	11300[a]	885
16553	604	11520	868

16559	604	11850	849
17144	583	12300	813
17780	562		

[a] Associated with MCD *A*-term

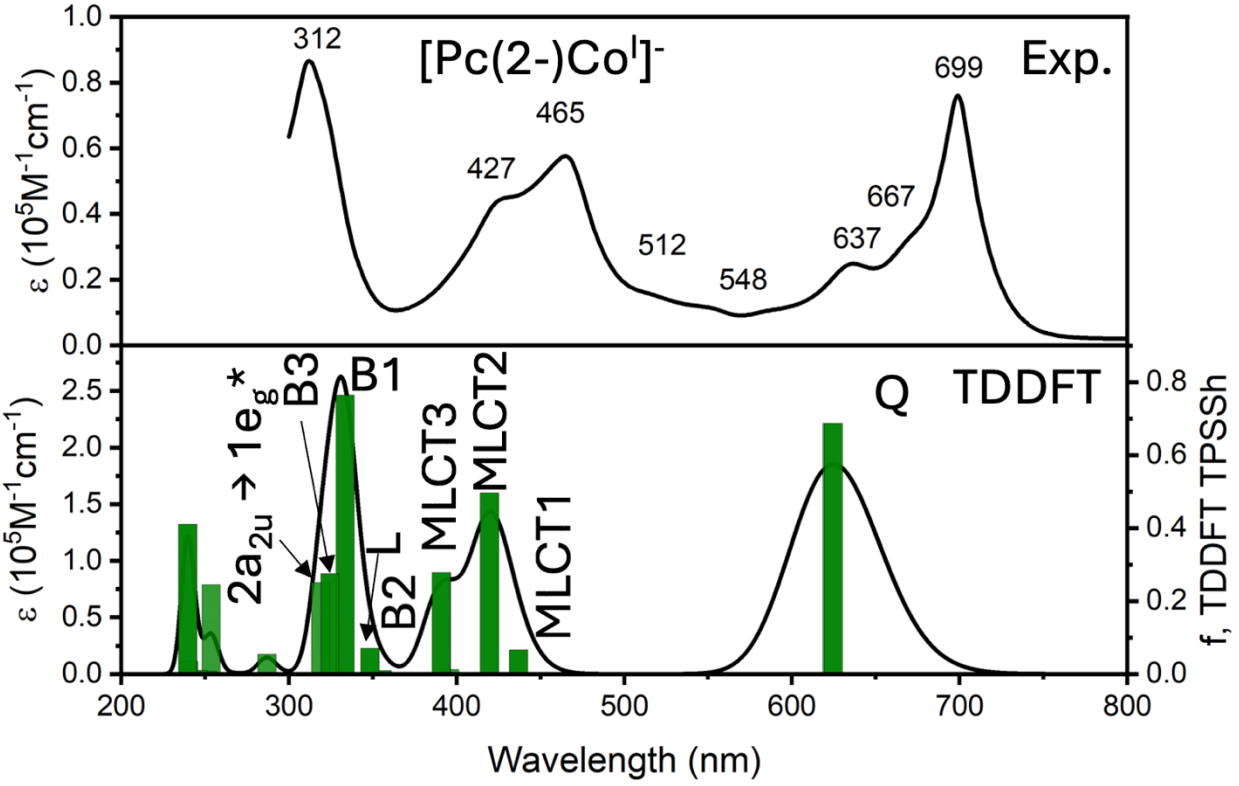

Figure 15. Experimental (top) *versus* TDDFT-predicted (bottom) UV-Vis spectra of $[Pc(2-)Co^{I}]^{-}$

.

In the case of $[Pc(2-)Co^{I}]^{-}$, one might expect that the occupied metal-centered orbitals will be strongly destabilized and located above or close to the phthalocyanine-centered $1a_{1u}$ orbital. Indeed, DFT predicts that the cobalt-centered d_{π} orbitals are HOMO and HOMO-1 in the $[Pc(2-)Co^{I}]^{-}$ anion, which are located in close proximity to the d_{z2} and $1a_{1u}$ orbitals (**Figure 8** and **Table 2**). These orbitals are ~1 eV less stable than the d_{xy} MO. The DFT-predicted LUMO and LUMO+1 are the classic Gouterman $1e_g$* pair,[132-134] which follows phthalocyanine-centered $1b_{1u}$*, $1b_{2u}$*, and $1a_{2u}$* orbitals. The energy difference between the LUMO/LUMO+1 pair and the cobalt-

centered b_{1g}* (d_{x2-y2}) orbital is ~2 eV, which excludes any symmetry-allowed LMCT transitions observed in the UV-Vis region. Such an electronic structure resembles Pc(2-)$Fe^{II}L_2$ complexes[112] to a large extent and implies the possibility of low-energy, symmetry-allowed MCLT transitions between cobalt-centered d_π orbitals and phthalocyanine-centered $1b_{1u}$*, $1b_{2u}$*, and $1a_{2u}$* orbitals. Indeed, these were predicted by Lever in 1985 based on his electrochemical potential approach.[113] TDDFT predicts the energies of the $d_\pi \rightarrow 1b_{1u}$*, $1b_{2u}$*, and $1a_{2u}$* MLCT1-3 transitions at 437, 420, and 391 nm respectively (**Figure 15** and **Table S3**). An additional MLCT transition dominated by the $d_{z2} \rightarrow 1a_{2u}$* single-electron excitation was predicted at 396 nm. Unlike the previously mentioned MLCT1-3, which should lead to three observable Faraday *A*-terms in the MCD spectrum of $[Pc(2-)Co^{I}]^-$, the latter MLCT transition is non-degenerate and should result in the observation of a MCD *B*-term. The MCD spectrum in the 400-550 nm region has at least three visible Faraday *A*-terms that could be associated with the TDDFT-predicted MLCT1-3 transitions. The last degenerate MLCT transition predicted by our TDDFT calculations was predicted at 240 nm and is dominated by the $d_\pi \rightarrow 2b_{2u}$* single-electron excitation. The phthalocyanine-centered π–π* transitions were predicted at 625 nm (Q-band, 98% $1a_{1u} \rightarrow 1e_g$*), 356 nm (B2-band, 87% $1b_{2u} \rightarrow 1e_g$*), 348 nm (L-band, 89% $1a_{1u} \rightarrow 2e_g$*), 334 nm (B1-band, 77% $1a_{2u} \rightarrow 1e_g$*), 324 nm (B3-band, 75% $1b_{1u} \rightarrow 1e_g$*), 319 nm (π–π*, 59% $2a_{2u} \rightarrow 1e_g$*), 287 nm (π–π*, 59% $2a_{1u} \rightarrow 1e_g$*), 252 nm (π–π*, 79% $1a_{1u} \rightarrow 3e_g$*), 246 nm (π–π*, 72% $1e_g \rightarrow 1b_{1u}$*), and 240 nm (π–π*, 84% $2e_g \rightarrow 1b_{1u}$*, **Table S3**). In general, our TDDFT calculations suggest that the ~380-550 nm spectral envelope should be dominated by MCLT transitions. Again, our TDDFT calculations predicted no symmetry-allowed transitions in the Q-band region except the Q-band. Thus, it is quite likely that the relatively strong MCD signal with positive amplitude observed at ~620 nm is reflective of the H-aggregation of the phthalocyanine chromophore.

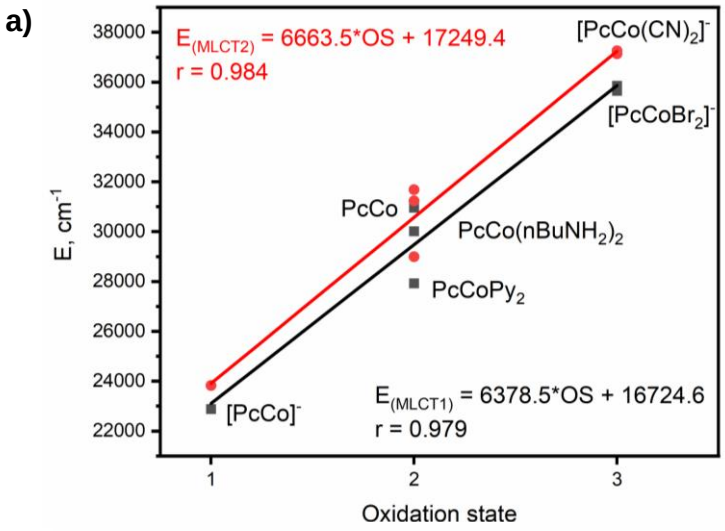
a)
E(MLCT2) = 6663.5*OS + 17249.4
r = 0.984
[PcCo(CN)2]-
[PcCoBr2]-
PcCo
PcCo(nBuNH2)2
PcCoPy2
[PcCo]-
E(MLCT1) = 6378.5*OS + 16724.6
r = 0.979
E, cm-1
Oxidation state

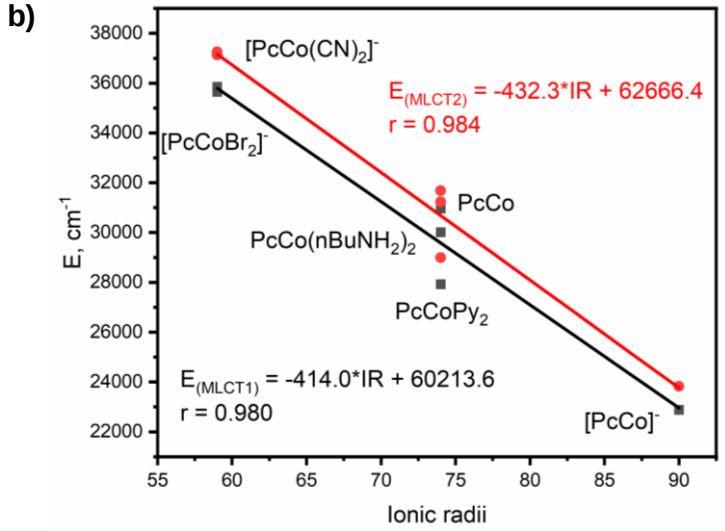
b)
[PcCo(CN)2]-
E(MLCT2) = -432.3*IR + 62666.4
r = 0.984
[PcCoBr2]-
PcCo
PcCo(nBuNH2)2
PcCoPy2
E(MLCT1) = -414.0*IR + 60213.6
r = 0.980
[PcCo]-
E, cm-1
Ionic radii

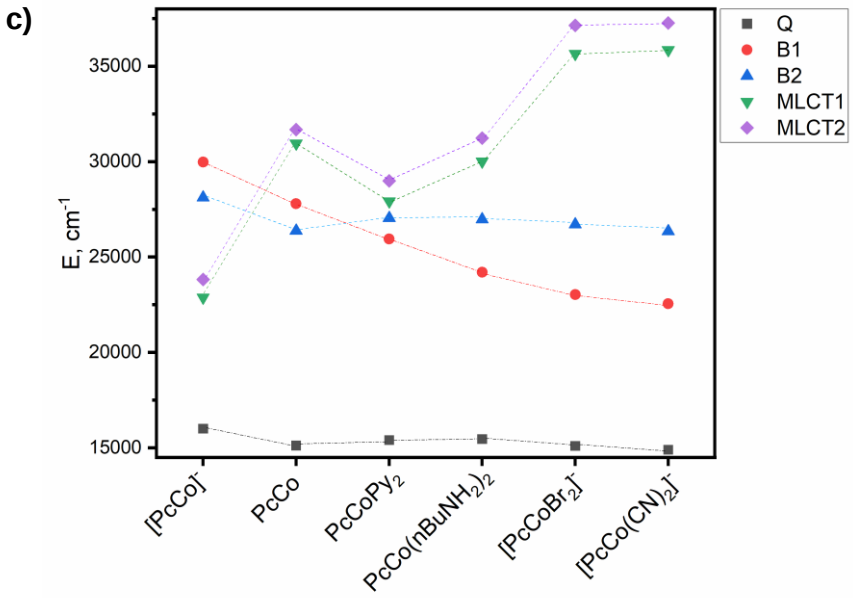
c)
Q
B1
B2
MLCT1
MLCT2
E, cm-1
[PcCo]-
PcCo
PcCoPy2
PcCo(nBuNH2)2
[PcCoBr2]-
[PcCo(CN)2]-

Figure 16. TDDFT-predicted energies of the MLCT1 and MLCT2 transitions *versus* cobalt oxidation state (a) and cobalt ionic radii (b). Selected transition energies of π–π* and charge-transfer transitions in cobalt phthalocyanines predicted by TDDFT calculations (c).

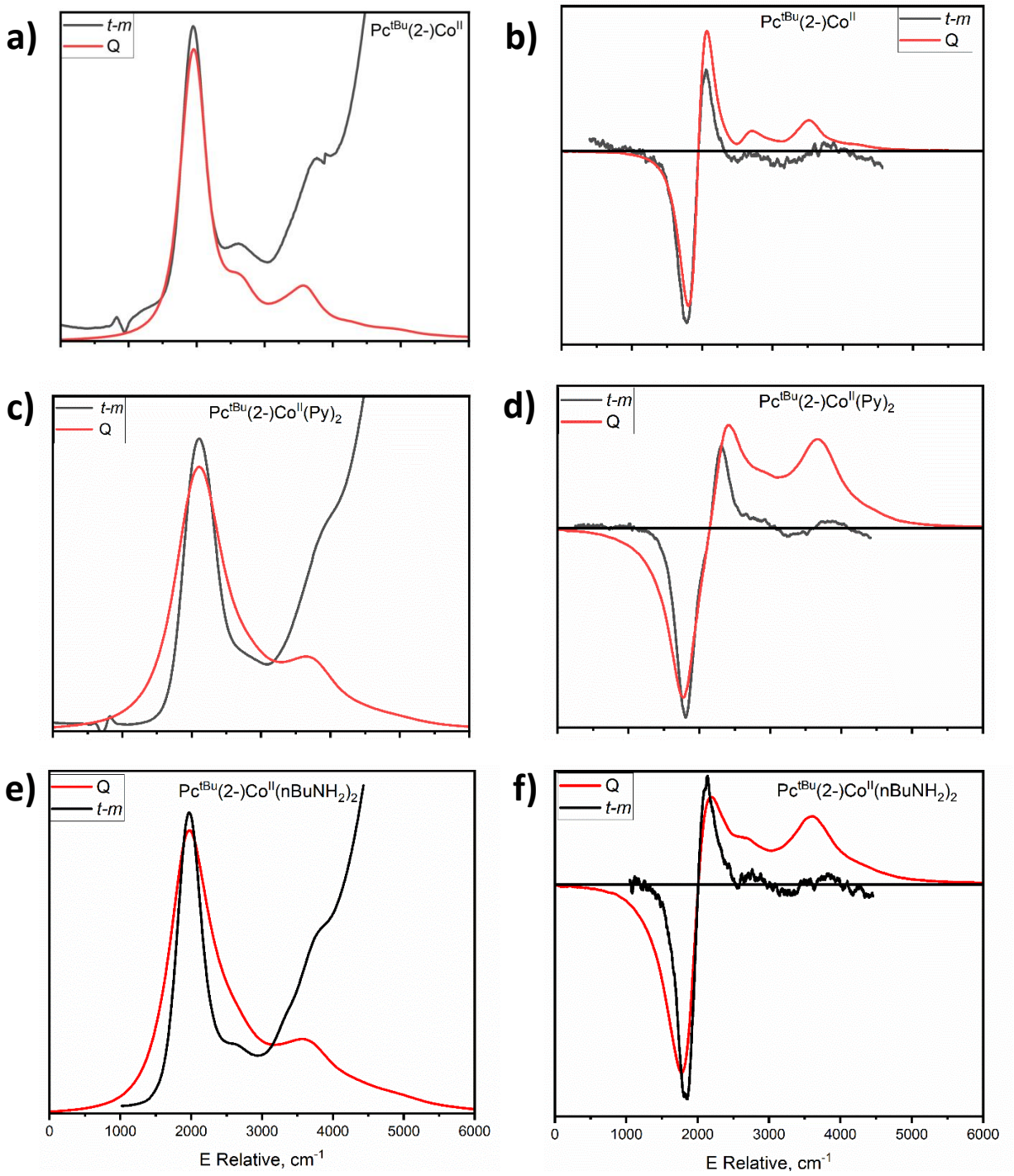

Figure 17. Overlays of absorption and MCD spectra in Q- and *t-m* bands regions: $Pc^{tBu}(2\text{-})Co^{II}$ complex (a and b), $Pc^{tBu}(2\text{-})Co^{II}Py_2$ complex (c and d), and $Pc^{tBu}(2\text{-})Co^{II}(n\text{BuNH}_2)_2$ (e and f).

The overall agreement between theoretically predicted and experimental UV-Vis-NIR spectra of cobalt phthalocyanines discussed in this report is very good (**Figures 13-15**). Indeed, TDDFT calculations correctly predicted the lack of intense transitions between the Q- and B-bands for cobalt(II) complexes and explained the nature of such transitions for cobalt(I) and cobalt(III) systems. They also predicted the presence of *t-m* transitions in the NIR region for cobalt(II) systems. The systematic increase of the B1-band energy from cobalt(I) to cobalt(III) systems is also correctly predicted by TDDFT calculations and reflects the systematic decrease of the $1a_{1u}$ - $1a_{2u}$ energy gap with increasing oxidation state of the central metal ion. TDDFT calculations also predicted oxidation state (or ionic radii) dependence on the energies of the MLCT1 and MLCT2 transitions in all cobalt complexes (**Figure 16**). Indeed, one might expect that upon increase of metal oxidation state, the cobalt-centered d_π orbitals will become more stable, and the relative energies of the phthalocyanine core will remain nearly constant. In this case, the energies of the MLCT1 and MLCT2 transitions will increase with increasing oxidation state. Analysis of the profiles of the Q- and *t-m* transitions is also interesting (**Figure 17**). In all cases, a close resemblance in the absorption spectra envelopes was observed, with the best match coming from the UV-Vis-NIR spectra of $Pc^{tBu}(2\text{-})Co^{II}$. The $Q_{0\text{-}0}$- and $t\text{-}m_{0\text{-}0}$ transitions are clearly associated with a MCD *A*-term. The presence of a second *A*-term for the $t\text{-}m_{0\text{-}2}$ transition was previously observed in copper phthalocyanine complexes.[94] The overlap of the UV-Vis-NIR and MCD spectra also suggests that the only difference upon axial ligand coordination is the broadening of the $Q_{0\text{-}0}$ band, which likely reflects the $Pc(2\text{-})Co^{II}L_2 \rightleftarrows Pc(2\text{-})Co^{II}L + L \rightleftarrows Pc(2\text{-})Co + L$ equilibria.

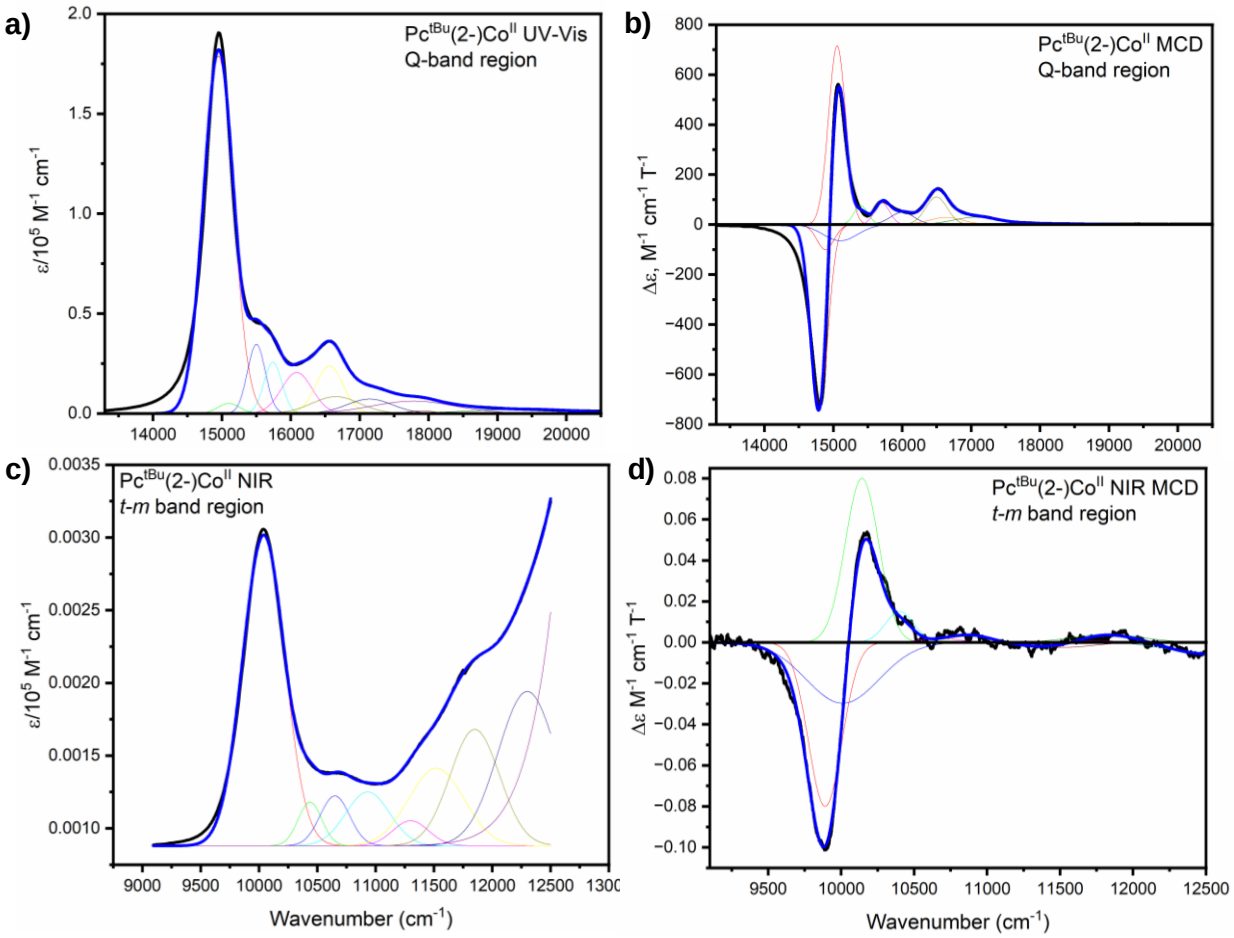

Figure 18. Band deconvolution of UV-Vis (a and c) and MCD (b and d) spectra of $Pc^{tBu}(2\text{-})Co^{II}$ in Q- (a and b) and *t-m* (c and d) spectral regions.

Band deconvolution analysis of the Q- and *t-m* spectral envelopes of $Pc^{tBu}(2\text{-})Co^{II}$ is shown in **Figure 18**. Similar to the copper(II) phthalocyanine complexes, it seems that the vibronic intervals for Q- and *t-m* sets are closely related (**Table 7**). The $Q_{0\text{-}0} - t\text{-}m_{0\text{-}0}$ energy difference for cobalt(II) phthalocyanines ranges between 4869 and 5134 cm^{-1}, which is slightly smaller than that observed in copper(II) phthalocyanines (5470-5585 cm^{-1}).[94] There has been a controversial discussion on the nature of the NIR bands in cobalt(II) phthalocyanines. Indeed, in a series of

reports, Cariati and co-workers assigned these bands to d-d transition,[86-89] while later Lever and co-workers assigned them as *t-m* bands.[90] Based on the discussion above and below, we are confident that the NIR bands observed in cobalt(II) phthalocyanines belong to the *t-m* transition and its vibronic components. First, as shown in **Figure 17**, the Q- and *t-m*-band region profiles are very similar, indicative of the close energy intervals for the vibronic components. Next, the molar extinction coefficients of the $t\text{-}m_{0\text{-}0}$ transitions (ε = 306-1443 M^{-1} cm^{-1}) are significantly higher than those expected for d-d transitions in centrosymmetric tetragonal cobalt complexes. Third, the energies of $t\text{-}m_{0\text{-}0}$ bands in both hexa- and tetra-coordinated cobalt(II) phthalocyanines range between 9815 and 10310 cm^{-1} (~500 cm^{-1} difference) for all complexes studied in this work. This range is even smaller for *tert*-butyl substituted compounds (9814-10040 cm^{-1}; ~240 cm^{-1} difference). Based on simple ligand-field theory considerations (which are obviously oversimplified but can be used to illustrate our point), one might expect a significantly larger energy difference for d-d transitions in tetra- and hexa-coordinate compounds. Indeed, following Lever[135] and Kida,[136] one might expect the state diagram shown in **Figure 19** for cobalt(II) ion in systems with D_{4h} symmetry. According to this diagram (ignoring quartet excited states, which should give negligible intensities of d-d transitions), three excited states might, potentially, be observed in the low-energy region. These are $^2B_{1g}$ ($d_{z2} \rightarrow d_{x2\text{-}y2}$ transition), ^2E_g ($d_{\pi} \rightarrow d_{z2}$ transition), and $^2B_{2g}$ ($d_{xy} \rightarrow d_{z2}$ transition) states. Out of these, only the ^2E_g excited state is degenerate and can lead to the observation of MCD *C*- or *A*-terms (a MCD *A*-term was always observed for the lowest energy NIR band in cobalt phthalocyanines). It is expected that the energy of the d_{z2} orbital will vary significantly in tetra- and hexa-coordinated cobalt(II) phthalocyanines. Its energy should also vary in hexa-coordinated complexes because of the differences in σ-donor strength between pyridine and *n*-butyl amine axial ligands. Indeed, it is clear from **Table 3** that d_{z2} orbital has the

largest energy influence by the axial ligands in cobalt(II) phthalocyanines compared to any other *d*-orbitals. Not surprisingly, the largest variation of the TDDFT-predicted energies of d-d transitions among Pc(2-)Co^{II}, Pc(2-)$Co^{II}Py_2$, and Pc(2-)$Co^{II}(n\text{BuNH}_2)_2$ were observed when the electron was transferred from or to the d_{z2} orbital (**Table 8**). For instance, TDDFT-predicted energies of the ^2E_g ($d_\pi \rightarrow d_{z2}$ transition) state are 5968, 16035, and 16776 cm^{-1} for Pc(2-)Co^{II}, Pc(2-)$Co^{II}Py_2$, and Pc(2-)$Co^{II}(n\text{BuNH}_2)_2$ complexes, respectively. Thus, TDDFT-predicted energies of this state vary significantly and are inconsistent with the nearly constant position of the lowest energy NIR band observed in cobalt(II) phthalocyanines. Similarly, TDDFT-predicted energies of the $^2B_{1g}$ ($d_{z2} \rightarrow d_{x2-y2}$ transition) excited state are 27925, 13572, and 11710 cm^{-1} for Pc(2-)Co^{II}, Pc(2-)$Co^{II}Py_2$, and Pc(2-)$Co^{II}(n\text{BuNH}_2)_2$, respectively. According to TDDFT calculations, the ^4E_g state should be observed close to the NIR region. However, it cannot be assigned to the NIR transitions observed in this region in cobalt(II) phthalocyanines because: (i) predicted energies for three different complexes still vary significantly (2474 cm^{-1}; ~0.3 eV); (ii) intensities of the quartet states should be negligibly small, while the observed intensities of the NIR transitions in cobalt(II) phthalocyanines were found between 306 and 1443 M^{-1} cm^{-1}. Finally, TDDFT-predicted energies for the ^2E_g state are between 25433 and 26434 cm^{-1}, ~2 eV higher in energy than the NIR bands observed in the cobalt(II) phthalocyanines. Although it is obvious that the TDDFT calculations have some errors and the predicted energies will have exchange-correlation functional dependency (TPSSh exchange-correlation functional is a good compromise for the accurate predictions of the π–π* and charge-transfer transitions), it is difficult to see that TDDFT calculations can result in ~2 eV errors for d-d transitions. Indeed, TDDFT-predicted 10*Dq* values for cobalt(II) phthalocyanines (**Table 8**) are in excellent agreement with the 10*Dq* values determined experimentally for Pc(2-)Co^{II}.[137,138] If our calculations are within the expected TDDFT errors (0.1-

0.2 eV), then some d-d transitions should be located in the NIR region with energies lower than the Q-band. However, taking into consideration the expected molar extinction coefficients for d-d transitions in centrosymmetric molecules (ε ~1-10 M^{-1} cm^{-1}; all cobalt(II) phthalocyanines discussed here have effective D_{4h} symmetry) versus the molar extinction coefficients for the Q-band (ε ~100000-200000 M^{-1} cm^{-1}) and *t*-*m* transitions (ε ~300-1450 M^{-1} cm^{-1}), it is difficult to believe that such weak bands would be clearly observable. In addition, TDDFT predicts only one excited state of ^2E_g symmetry for Pc(2-)Co^{II} complex in the NIR region and no excited states of ^2E_g symmetry in this region for the axially coordinated systems. This contradicts the observation of the MCD *A*-term at ~1000 nm for Pc^{R4}(2-)Co^{II}, Pc^{R4}(2-)$Co^{II}Py_2$, and Pc^{R4}(2-)Co^{II}(*n*$BuNH_2)_2$. Of course, because of covalency, d-orbitals in cobalt phthalocyanines have significant contributions from the ligand and thus, TDDFT-predicted d-d transitions are not classic crystal field transitions. Nevertheless, overall, the data and discussion above suggest that the NIR bands observed in cobalt(II) phthalocyanines are *t*-*m* in nature and cannot be assigned to d-d transitions.

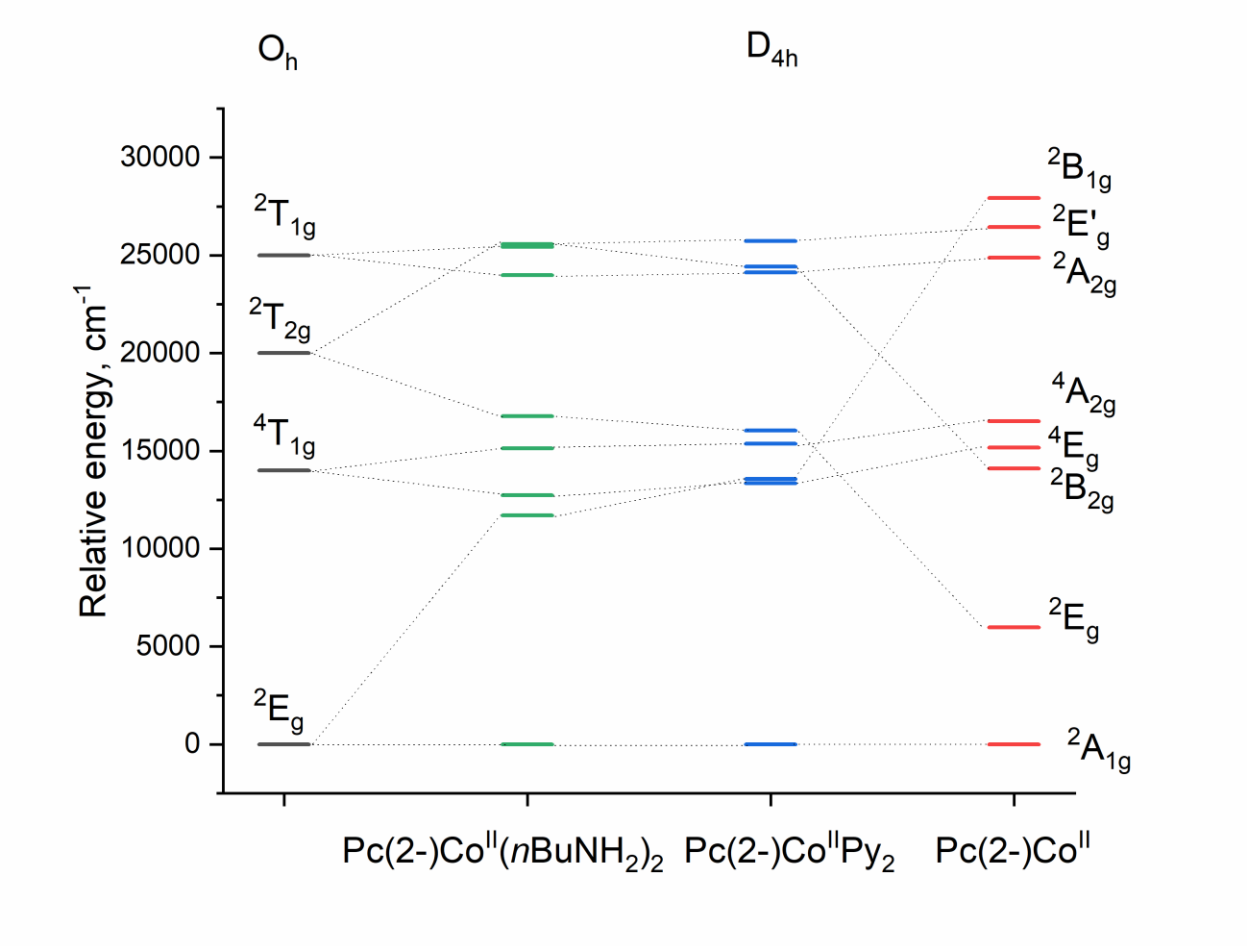

Figure 19. Term splitting diagram and TDDFT-predicted low-energy d-d transitions in cobalt(II) phthalocyanines in D_{4h} effective symmetry.

Table 8. TDDFT-predicted predominant d-d transitions in cobalt(II) phthalocyanines.[a]

	Pc(2-)Co^{II}			Pc(2-)$Co^{II}Py_2$			Pc(2-)$Co^{II}(n BuNH_2)_2$		
ES symm	E, cm^{-1} (λ, nm)	$<S^2>$	Composition[b]	E, cm^{-1} (λ, nm)	$<S^2>$	Composition[b]	E, cm^{-1} (λ, nm)	$<S^2>$	Composition[b]
^2E_g	5968 (1676)	0.771	92.0% H-2(β) → L+2(β)	16035 (623)	0.831	76.6% H-1(β) → L+9(β)	16743 (597)[c]	0.823	76.5% H-1(β) → L+7(β)
	5968 (1676)	0.771	92.0% H-1(β) → L+2(β)	16035 (623)	0.831	76.6% H-2(β) → L+9(β)	16810 (595)[c]	0.822	76.0% H-2(β) → L+7(β)
$^2B_{2g}$	14106 (709)	0.901	73.6% H-3(β) → L+2(β), 10.2% H-12(β) → L+2(β)	24422 (409)	0.831	79.9% H-3(β) → L+9(β)	25569 (391)	0.941	68.0% H-3(β) → L+7(β)
^4E_g	15164 (659)	2.696	50.7% H-1(α) → L+2(α), 31.2% H-1(β) → L+5(β), 13.7% H-11(α) → L+2(α)	13346 (749)	2.422	44.2% H-2(α) → L+2(α), 21.5% H-1(β) → L+12(β), 16.2% H-1(α) → L+1(α), 11.0% H-1(β) → L+10(β)	12690 (788)[c]	2.552	32.7% H-2(α) → L+2(α), 25.0% H-1(β) → L+8(β), 14.1% H-1(β) → LUMO(β), 13.4% H-2(β) → L+1(β)
	15164 (659)	2.696	50.7% H-2(α) → L+2(α), 31.2% H-2(β) → L+5(β), 13.7% H-12(α) → L+2(α)	13346 (749)	2.422	44.2% H-3(α) → L+2(α), 21.5% H-2(β) → L+12(β), 16.2% H-1(α) → LUMO(α), 11.0% H-2(β) → L+10(β)	12765 (783)[c]	2.690	50.3% H-3(α) → L+2(α), 38.8% H-2(β) → L+8(β)
$^4A_{2g}$	16513 (606)	2.748	45.0% H-3(β) → L+5(β), 28.5% H-4(α) → L+2(α), 21.9% H-16(α) → L+2(α)	15361 (737)	2.742	32.0% H-3(β) → L+12(β), 28.0% H-4(α) → L+2(α), 16.2% H-18(α) → L+2(α), 16.1% H-3(β) → L+10(β)	15120 (661)	2.751	48.7% H-3(β) → L+8(β), 36.8% H-5(α) → L+2(α)
$^2A_{2g}$[d]	24879 (402)	0.768	42.1% H-3(β) → L+5(β), 36.3% H-	24117 (415)	0.776	32.5% H-4(α) → L+2(α), 29.2% H-	23982 (417)	0.767	45.0% H-3(β) → L+8(β), 40.5% H-5(α)

			4(α) → L+2(α), 15.5% H-16(α) → L+2(α)			3(β) → L+12(β), 15.8% H-3(β) → L+10(β), 11.5% H-18(α) → L+2(α)			→ L+2(α), 10.4% H-16(α) → L+2(α)
$^2E'_g$	26434 (378)	0.816	48.7% H-2(β) → L+5(β), 32.3% H-2(α) → L+2(α)	25727 (389)	0.839	25.9% H-2(α) → L+2(α), 25.9% H-1(β) → L+12(β), 16.3% H-1(β) → L+10(β)	25410 (394)[c]	0.819	41.7% H-1(β) → L+8(β), 24.9% H-2(α) → L+2(α)
	26434 (378)	0.816	48.7% H-1(β) → L+5(β), 32.3% H-1(α) → L+2(α)	25727 (389)	0.839	25.9% H-3(α) → L+2(α), 25.9% H-2(β) → L+12(β), 16.3% H-2(β) → L+10(β)	25456 (393)[c]	0.815	42.5% H-2(β) → L+8(β), 25.5% H-3(α) → L+2(α)
$^2B_{1g}$	27925 (358)	0.778	83.0% H-10(α) → L+2(α)	13572 (736)	1.091	57.0% H-1(α) → L+2(α), 20.1% H-1(β) → L+1(β), 20.1% H-2(β) → LUMO(β)	11710 (854)	0.834	81.0% HOMO(α) → L+2(α)

[a] Effective D_{4h} symmetries are used for Pc(2-)$Co^{II}Py_2$ and Pc(2-)$Co^{II}(n\text{BuNH}_2)_2$ complexes; [b] Only expansion coefficients with more than 10% contribution are shown; [c] Nearly degenerate states in C_i symmetry; [d] $10Dq$ = 3.08, 2.99, and 2.97 eV for Pc(2-)Co^{II}, Pc(2-)$Co^{II}Py_2$, and Pc(2-)$Co^{II}(n\text{BuNH}_2)_2$, respectively. Experimentally observed $10Dq$ for Pc(2-)Co^{II} complex are: 3.09 and 2.8 eV.[137,138]

The EPR $g_{\parallel}$ and $g_{\perp}$ values in cobalt(II) complexes with $(d_{xy})^2(d_{xz,yz})^4(d_{z2})^1$ configuration can be estimated on from ligand-field theory using Equations 1 and 2:[136,139-141]

$$g_{\parallel} = 2.0 \quad (1)$$

$$g_{\perp} = 2 - 6(\xi/\Delta E_{dxz,yz \rightarrow dz2}) \quad (2)$$

Here, ξ is a spin-orbit coupling constant for cobalt(II) ion in coordination compound and $\Delta E_{dxz,yz \rightarrow dz2}$ is the experimental or theoretically predicted energy of the $^2E_g \leftarrow {}^2A_{1g}$ ($d_{xz,yz} \rightarrow d_{z2}$) d-d transition. Following Kida,[136] we used ξ = -510 cm^{-1} TDDFT-predicted energies listed in **Table 8** for $^2E_g \leftarrow {}^2A_{1g}$ ($d_{xz,yz} \rightarrow d_{z2}$) d-d transitions for Pc(2-)Co^{II}, Pc(2-)$Co^{II}Py_2$, and Pc(2-)$Co^{II}(n\text{BuNH}_2)_2$. The calculated values for $g_{\perp}$ (2.51, 2.19, and 2.18 for Pc(2-)Co^{II}, Pc(2-)$Co^{II}Py_2$, and Pc(2-)$Co^{II}(n\text{BuNH}_2)_2$, respectively follow the experimental trend for $g_{\perp}$ values observed in Pc^{tBu}(2-)Co^{II}, Pc^{tBu}(2-)$Co^{II}Py_2$, and Pc^{tBu}(2-)$Co^{II}(n\text{BuNH}_2)_2$ and are in reasonable agreement with the experimental data. This, again, suggests that the energies of the $^2E_g \leftarrow {}^2A_{1g}$ ($d_{xz,yz} \rightarrow d_{z2}$) d-d transitions in Pc(2-)Co^{II}, Pc(2-)$Co^{II}Py_2$, and Pc(2-)$Co^{II}(n\text{BuNH}_2)_2$ should be quite different and thus NIR bands observed in cobalt(II) phthalocyanines cannot be assigned as d-d in nature. We also calculated the EPR parameters of Pc(2-)Co^{II}, Pc(2-)$Co^{II}Py_2$, and Pc(2-)$Co^{II}(n\text{BuNH}_2)_2$ using DFT methodology, with results shown in **Table 1** and Supporting Information Table S4. Since EPR spectroscopy is used in this report only for confirmation of the low-spin (s = 1/2) electronic structure of the cobalt(II) systems, detailed discussion on the influence of the exchange-correlation functionals[142] and basis sets[143] is relegated to the Supporting Information. In short, as one can see from **Table 1** and Supporting Information **Table S4**, we obtained good agreement between theory

and experiment for *g*-values. Trends in *A*-values are also correct for most tested functionals, although their absolute values differ significantly, indicating that a new computational protocol should be developed to accurately predict both, *g*- and *A*-values in phthalocyanine cobalt(II) systems. Nevertheless, our DFT calculations on the EPR parameters solidify our assumption that these compounds have low-spin configurations and the d_{z2} orbital in the EPR active space (Supporting Information **Figure S12**).

Conclusions

In this report, we provided combined experimental (UV-Vis-NIR and MCD) and theoretical (DFT and TDDFT) analyses of the optical and magnetooptical properties of cobalt(I), cobalt(II), and cobalt(III) phthalocyanines between 250 and 1200 nm. Two cobalt(I), five cobalt(II), and two cobalt(III) complexes were studied. It was shown that diamagnetic systems have no activity in the NIR spectral envelope, while paramagnetic low-spin cobalt(II) phthalocyanines have an easily detectable set of NIR bands. The NIR *t-m* bands in $Pc^{R4}(2\text{-})Co^{II}L_2$ (L = nil, Py, or *n*$BuNH_2$; R = H or *tert*-Bu) complexes were studied by MCD spectroscopy for the first time and compared to those reported earlier by us in $Pc^{R4}(2\text{-})Cu$ (R = *tert*-Bu or SO_3Na) compounds. In all cases, the Faraday MCD *A*-term was observed for the lowest energy NIR transition. Based on their profile similarities with the Q-band, degeneracy of the lowest energy MCD signal, intensities, TDDFT calculations, and ligand-field theory considerations, the NIR transitions can be assigned to *t-m* transitions with a high degree of confidence. We also showed that the MLCT bands in cobalt phthalocyanine complexes increase in energy going from cobalt(I) to cobalt(III) systems in a stepwise fashion. DFT and TDDFT calculations also confirm and explain changes in energies of the B1-band going from cobalt(I) to cobalt(III) complexes. Additional absorption bands observed in the 370-530 nm

spectral envelope in $[Pc^{R4}(2\text{-})Co^{III}X_2]^-$ complexes (X = Br^- or CN^-) were also assigned with a high level of confidence for the first time. This work provides the first combined systematic experimental and theoretical study that highlights similarities and differences in (magneto)optical spectroscopy of cobalt phthalocyanines spanned over three oxidation states at the central metal ion.

Experimental Section

Materials and Instrumentation

All solvents were purified using standard procedures. $Pc(2\text{-})Co^{II}$ was purchased from Alfa Aesar. Pyridine, $[NBu_4]Br$, and $[NBu_4](CN)$ were purchased from Aldrich. N-butylamine and bromine were purchased from Thermo Fisher Scientific. $Pc^{tBu}(2\text{-})Co^{II}$ was synthesized as previously described.[102] Reduction of $Pc(2\text{-})Co^{II}$ to $[Pc(2\text{-})Co^{I}]^-$ was carried out in DMF following the previously published procedures.[100,106] Formation of $(NBu)_4[Pc(2\text{-})Co^{III}(CN)_2]^-$ was performed in DMF using excess $[NBu_4](CN)$.[103] $Pc^{Rn}(2\text{-})Co^{II}(n\text{BuNH}_2)_2$ complexes were synthesized by dissolving $Pc^{Rn}(2\text{-})Co^{II}$ complexes in DCM in the presence of a large (~1000 times) of *n*-butylamine. $Pc^{Rn}(2\text{-})Co^{II}(Py)_2$ complexes were formed by dissolving $Pc^{Rn}(2\text{-})Co^{II}$ in pyridine. $(NBu_4)[Pc^{tBu}(2\text{-})Co^{III}Br_2]$ complex was prepared by adding 1.1 eq of the Br_2 in DCM to the DMF solution of the $Pc^{tBu}(2\text{-})Co^{II}$ in 0.1 M of $[NBu_4]Br$. In all cases, the UV-Vis-NIR spectra of the target compounds were identical to those reported earlier.

All spectra were collected using a Q-3 quartz cell purchased from Labomed Inc. UV-Vis data were collected on a JACSO V-770 spectrometer and MCD data were recorded using a JASCO V-1500 spectropolarimeter with a permanent 1.6 T magnet. Each MCD sample was recorded three

times each with a parallel and anti-parallel field. All intensities of MCD data are expressed in molar ellipticity per tesla. Origin Pro 8.0[144] was used for simultaneous band deconvolution analysis of the UV-Vis-NIR and MCD spectra of $Pc^{tBu}(2\text{-})Co^{II}$. EPR spectra were collected on a Bruker X-band ELEXSYS E-500 instrument at 150 K. Samples were prepared and frozen under a nitrogen atmosphere. Toluene was used for $Pc^{tBu}(2\text{-})Co^{II}$ and toluene/axial ligand (50/50 v/v) was used for $Pc^{tBu}(2\text{-})Co^{II}(Py)_2$ and $Pc^{tBu}(2\text{-})Co^{II}(n\text{BuNH}_2)_2$.

DFT and TDDFT calculations

All calculations were performed using Gaussian 16.[145] TPSSh[146,147] (hybrid functional with 10% of Hartree-Fock exchange) was used for all geometry optimizations, TDDFT, and single-point DFT calculations to better describe charge-transfer transitions compared to GGA exchange-correlation functionals. Wachter's full-electron basis set[148] for cobalt and the 6-311G(d) basis set[149] for all other atoms were used. PCM[150] using the dielectric constant of DMF was used to mimic solvent effects in the systems. Geometries of $PcCo^{II}$, $[PcCo^{I}]^-$, $[PcCo^{III}Br_2]^-$, and $[PcCo^{III}(CN)_2]^-$ converged to the D_{4h} point group, $PcCo^{II}Py_2$ converged to the D_{2d} point group, and $PcCo^{II}(\boldsymbol{n}\text{BuNH}_2)_2$ converged to the C_i point group. Frequencies were calculated for each converged structure to ensure that the structure converged to a minimum. GaussView 6.0 was used for MO visualization and QMForge[151] for orbital composition analysis.

ASSOCIATED CONTENT

Supporting Information

The Supporting Information is available free of charge. Additional UV-Vis-NIR spectra and DFT and TDDFT information (PDF).

AUTHOR INFORMATION

Corresponding Authors

Christopher J. Ziegler - Department of Chemistry, University of Akron, Akron, Ohio 44325, United States; orcid.org/ORCID: 0000-0002-0142-5161; Email: ziegler@uakron.edu

Brendon J. McNicholas - Department of Chemistry, University of Tennessee, Knoxville, Tennessee 37996, United States; orcid.org/0000-0002-3654-681X; Email: bmcnicho@utk.edu

Victor N. Nemykin – Department of Chemistry, University of Tennessee, Knoxville, Tennessee 37996, United States; orcid.org/0000-0003-4345-0848; Email: vnemykin@utk.edu

Authors

Breanna E. Muldowney - Department of Chemistry, University of Tennessee, Knoxville, Tennessee 37996, United States

Dustin E. Nevonen – Department of Chemistry, University of Tennessee, Knoxville, Tennessee 37996, United States

Towhidi Illius Jeaydi – Department of Chemistry, University of Akron, Akron OH 44325, United States

Notes

The authors declare no competing financial interest.

ACKNOWLEDGMENTS

Generous support from the NSF(CHE-2153081), Minnesota Supercomputing Institute, and the University of Tennessee to V.N. is greatly appreciated. B.J.M. acknowledges generous support from the University of Tennessee. BEM is a recipient of the fellowship provided by the NSF - Division of Graduate Education (grant #2152168). We wish to acknowledge Katelyn Llewellyn for her help with some data collection.

References

1. P. Gregory, *J. Porphyrins Phthalocyanines*, 2000, **4**, 432-437. DOI: 10.1002/(SICI)1099-1409(200006/07)4:4<432::SID-JPP254>3.0.CO;2-N.

2. S. Q. Lomax, *Studies in Conservation*, 2005, **50**, 19-29, DOI: 10.1179/sic.2005.50.Supplement-1.19.

3. S. Benkhaya, S. M'rabet and A. El Harfi, *Inorg. Chem. Commun.,* 2020, **115**, 107891, DOI: 10.1016/j.inoche.2020.107891.

4. A. B. Sorokin, *Chem. Rev.,* 2013, **113**, 8152-8191, DOI: 10.1021/cr4000072.

5. P. Afanasiev, and A. B. Sorokin, *Acc. Chem. Res.*, 2016, **49**, 583-593, DOI: 10.1021/acs.accounts.5b00458.

6. D. Wöhrle, N. Baziakina, O. Suvorova, S. Makarov, V. Kutureva, E. Schupak, and G. Schnurpfeil, *J. Porphyrins Phthalocyanines,* 2004, **8**, 1390-1401, DOI: 10.1142/S1088424604000751.

7. L. P. Cailler, M. Clemancey, J. Barilone, P. Maldivi, J. M. Latour, and A. B. Sorokin, *Inorg. Chem.,* 2020, **59**, 1104-1116, DOI: 10.1021/acs.inorgchem.9b02718.

8. C. Colomban, A. H. Tobing, G. Mukherjee, C. V. Sastri, A. B. Sorokin, and S. P. de Visser, *Chem. Eur. J.*, 2019, **25**, 14320-14331, DOI: 10.1002/chem.201902934.

9. H. M. Neu, V. V. Zhdankin, and V. N. Nemykin, *Tetrahedron Lett.*, 2010, **51** 6545-6548, DOI: 10.1016/j.tetlet.2010.10.023.

10. H. M. Neu, M. S. Yusubov, V. V. Zhdankin, and V. N. Nemykin, *Adv. Synth. Catal.*, 2009, **351**, 3168-3174, DOI: 10.1002/adsc.200900705.

11. I. M. Geraskin, M. W. Luedtke, H. M. Neu, V. N. Nemykin, and V. V. Zhdankin, *Tetrahedron Lett.*, 2008, **49**, 7410-7412, DOI: 10.1016/j.tetlet.2008.10.060.

12. J. R. Griffin, C. I. Wendell, J. A. Garwin, and M. C. White, *J. Am. Chem. Soc.*, 2017, 1**39**, 13624-13627, DOI: 10.1021/jacs.7b07602.

13. P. Hu, M. Tan, L. Cheng, H. Zhao, R. Feng, W. J. Gu, and W. Han, *Nature Commun.*, 2019, **10**, 1-9, DOI: 10.1038/s41467-019-10414-7.

14. C. J. P. Monteiro, M. A. F. Faustino, M. G. P. M. S. Neves, M. M. Q. Simoes, and E. Sanjust, *Catalysts*, 2021, **11**, 122, DOI: 10.3390/catal11010122.

15. E. N. Carrion, A. Loas, H. H. Patel, M. Pelmus, K. Ramji, and S.M. Gorun, *Journal of Porphyrins and Phthalocyanines*, 2018, **22**, 371-397, DOI: 10.1142/S1088424618500189.

16. D. Wöhrle, O. Suvorova, R. Gerdes, O. Bartels, L. Lapok, N. Baziakina, S. Makarov, and A. Slodek, *J. Porphyrins Phthalocyanines*, 2004, **8**, 1020-1041, DOI: 10.1142/S1088424604000398.

17. O. L. Kaliya, E. A. Lukyanets, and G. N. Vorozhtsov, *J. Porphyrins Phthalocyanines*, 1999, **3**, 592-610, DOI: 10.1002/(SICI)1099-1409(199908/10)3:6/7<592:;AID-JPP180>3.0.CO;2-G.

18. D. Wöhrle, O. Suvorova, R. Gerdes, O. Bartels, L. Lapok, N. Baziakina, S. Makarov, and A. Slodek, *J. Porphyrins Phthalocyanines*, 2004, **8**, 1020-1041, DOI: 10.1142/S1088424604000398.

19. G. F. Manbeck, and E. Fujita, *J. Porphyrins Phthalocyanines*, 2015, **19**, 45-64, DOI: 10.1142/S1088424615300013.

20. B. Domingo-Tafalla, T. Chatterjee, and E. Palomares, *J. Porphyrins Phthalocyanines*, 2023, **27**, 23-46, DOI: 10.1142/S1088424623300033.

21. C. He, Z. Y. Wu, L. Zhao, M. Ming, Y. Zhang, Y. Yi, and J. S. Hu, *ACS Catalysis*, 2019, **9**, 7311-7317, DOI: 10.1021/acscatal.9b00959.

22. J. Govan, G. Abarca, C. Aliaga, B. Sanhueza, W. Orellana, G. Cardenas-Jiron, J. H. Zagal, and F. Tasca, *Electrochem. Commun.*, 2020, **118**, 106784, DOI: 10.1016/j.elecom.2020.106784.

23. R. Praats, M. Kaarik, A. Kikas, V. Kisand, J. Aruvali, P. Paiste, M. Merisalu, J. Leis, V. Sammelselg, J. H. Zagal, S. Holdcroft, N. Nakashima, and K. Tammeveski, *Electrochim. Acta*, 2020, **334,** 135575, DOI:10.1016/j.electacta.2019.135575.

24. F. J. Recio, C. A. Gutierrez, R. Venegas, C. Linares-Flores, C. A. Caro, and J. H. Zagal, *Electrochim. Acta*, 2014, **140,** 482-488, DOI: 10.1016/j.electacta.2014.04.098.

25. L. Xie, Y. Wang, Q. Kong, and R. Cao, *ChemCatChem*, 2024, **16**, e202400956, DOI: 10.1002/cctc.202400956.

26. J. Masa, K. Ozoemena, W. Schuhmann, and J. H. Zagal, *J. Porphyrins Phthalocyanines*, 2012, **16**, 761-784, DOI: 10.1142/S1088424612300091.

27. A. B. P. Lever, *J. Porphyrins Phthalocyanines*, 1999, **3**, 488-499, DOI: 10.1002/(SICI)1099-1409(199908/10)3:6/7<488::AID-JPP167>3.0.CO;2-K.

28. Y. H. Tse, P. Janda, H. Lam, J. Zhang, W. J. Pietro, and A. B. P. Lever, *J. Porphyrins Phthalocyanines*, 1997, **1**, 3-16, DOI: 10.1002/(SICI)1099-1409(199701)1:1<3::AID-JPP1>3.0.CO;2-V.

29. S. Sajid, S. Alzahmi, I. B. Salem, J. Park, and I. M. Obaidat, *J. M. T. Ener.*, 2023, **37**, 101378, DOI: 10.1016/j.mtener.2023.101378.

30. X. Li, and J. Cao, *Science Bulletin*, 2020, **65**, 1688-1690, DOI: 10.1016/j.scib.2020.06.032.

31. D. Molina, J. Follana-Berna, and A. Sastre-Santos, ***J. Mater. Chem. C***, 2023, **11**, 7885-7919, DOI: 10.1039/D2TC04441B.

32. M. Gsaenger, D. Bialas, L. Huang, M. Stolte, and F. Wuerthner, *Adv. Mater*, 2016, **28**, 3615-3645, DOI: 10.1002/adma.201505440.

33. J. Labella, J. Laforga-Martin, and T. Torres, *CCS Chem.*, 2024, **6**, 276-296, DOI: 10.31635/ccschem.023.202303395.

34. G. Bottari, G. de la Torre, D. M. Guldi, and T. Torres, *Coord. Chem. Rev.*, 2021, **428**, 213605, DOI: 10.1016/j.ccr.2020.213605.

35. P. Ona-Burgos, M. Casimiro, I. Fernandez, A. V. Navarro, J. F. Fernandez-Sanchez, A. S. Carretero, and A. F. Gutierrez, *Dalton Trans.*, 2010, **39**, 6231-6238, DOI: 10.1039.B924429H.

36. A. Valero-Navarro, J. F. Fernandez-Sanchez, A. Segura-Carretero, U. E.Spichiger-Keller, A. Fernandez-Gutierrez, P. Ona, and I. Fernandez, *J. Porphyrins Phthalocyanines*, 2009, **13**, 616-623, DOI: 10.1142/S1088424609000796.

37. J. F. Fernandez-Sanchez, I. Fernandez, R. Steiger, R. Beer, R. Cannas, and U. E. Spichiger-Keller, *Adv. Functional Mater.*, 2007, **17**, 1188-1198, DOI: 10.1002/adfm.200600428.

38. E. Demir, H. Silah, and B. Uslu, *Crit. Rev. Anal. Chem.*, 2022, **52**, 425-461, DOI: 10.1080/10408347.2020.1806702.

39. D. Klyamer, R. Shutilov, and T. Basova, *Sensors*, 2022, **22**, 895, DOI: 10.3390/s22030895.

40. R. J. Mortimer, *Chem. Soc. Rev.*, 1997, **26**, 147-156, DOI: 10.1039/CS9972600147.

41. E. A. Lukyanets, *J. Porphyrins Phthalocyanines*, 1999, **3**, 424-432, DOI: 10.1002/(sici)1099-1409(199908/10)3:6/7<424::aid-jpp151>3.0.co;2-k.

42. E. A. Lukyanets, and V. N. Nemykin, *J. Porphyrins Phthalocyanines*, 2010, **14** , 1-40, DOI: 10.1142/S1088424610001799.

43. M. Wainwright, Photoantivirals in blood disinfection, *Trends Photochem. Photobiol.*, 2001, **8**, 97-106.

44. I. J. MacDonald, and T. J. Dougherty, *J. Porphyrins Phthalocyanines*, 2001, **5**, 105-129, DOI: 10.1002/jpp.328.

45. C. M. Allen, W. M. Sharman, and J. E. Van Lier, *J. Porphyrins Phthalocyanines*, 2001, **5**, 161-169, DOI: 10.1002/jpp.324.

46. R. K. Pandey, *J. Porphyrins Phthalocyanines*, 2000, **4**, 368-373, DOI: 10.1002/(SICI)1099-1409(200006/07)4:4<368::AID-JPP244>3.0CO;2-6.

47. A. B. Dominguez, D. Ziental, J. Dlugaszewska, L. Sobotta, T. Torres, and M. S. Rodriguez-Morgade, *Eur. J. Med. Chem.*, 2025, **285**, 117214, DOI: 10.1016/j.ejmech.2024.117214.

48. B. H. Lessard, *ACS Appl. Electron. Mater*., 2024, **6**, 3006-3012, DOI:10.1021/acsaelm.4c0033.

49. H. Eichhorn, *J. Porphyrins Phthalocyanines*, 2000, **4**, 88-102, DOI: 10.1002/(SICI)1099-1409(200001/02)4:1<88::AID-JPP208>3.0.CO;2-6.

50. H. Engelkamp, and R. J. M. Nolte, *J. Porphyrins Phthalocyanines*, 2000, **4**, 454-459, DOI: 10.1002/1009-1409(200008)4:5<454::AID-JPP261>3.0.CO;2-D.

51. N. R. Armstrong, *J. Porphyrins Phthalocyanines*, 2000, **4**, 414-417, DOI: 10.1002(SICI)1099-1409(200006/07)4:4<414::AID-JPP247>3.0.CO;2-B.

52. H. Yu, J. Chen, X. Chen, T. Zhang, Y. Li, K. Chen, Y. Peng, and L. Chen, *Front bioeng biotechnol.*, 2023, **11**, 1181448, DOI: 10.3389/fbioe.2023.1181448.

53. H. Isago, H. Fujita, and T. Sugimori, *J. Inorg. Biochem.*, 2018, **180**, 222-229, DOI: 10.1016/j.jinorgbio.2017.12.014.

54. A. K. Mutyala, and J. S. Park, *Tetrahedron Lett.,* 2016, **57**, 1109-1112, DOI: 10.1016/j.tetlet.2016.01.098.

55. V. N. Nemykin, A. E. Polshyna, S. A. Borisenkova, and V. V. Strelko, *J. Mol. Cat. A: Chem*, 2007, **264**, 103-109, DOI: 10.1016/j.molcata.2006.08.093.

56. Z. Cheng, M. Dai, X. Quan, S. Li, D. Zheng, Y. Liu, and R. Yao, *J. Porphyrins Phthalocyanines*, 2019, **23**, 267-278, DOI: 10.1142/S108842461950010X.

57. A. Vashurin, A. Filippova, S. Znoyko, A. Voronina, O. Lefedova, I. Kuzmin, V. Maizlish, and O. Koifman, *J. Porphyrins Phthalocyanines*, 2015, **19**, 983-996, DOI: 10.1142/S1088424615500753.

58. A. Vashurin, I. Kuzmin, M. Razumov, S. Pukhovskaya, O. Golubchikov, A. Voronina, G. Shaposhnikov, and O. Koifman, *J. Porphyrins Phthalocyanines*, 2015, **19**, 1159-1167, DOI: 10.1142/S1088424615500911.

59. G. Das, B. Sain, and M. O. Garg, *Chemical Industry Digest*, 2012, **25**, 58-64.

60. J. K. Joseph, S. L. Jain, and B. Sain, *Ind. Eng. Chem. Res.* 2010, **49**, 6674-6677, DOI: 10.1021/ie100351s.

61. E. M. Tyapochkin, and E. I. Kozliak, *J. Mol. Cat. A: Chem.*, 2005, 2**42**, 1-17, DOI: 10.1016/j.molcata.2005.07.008.

62. E. M. Tyapochkin, and E. I. Kozliak, *J. Porphyrins Phthalocyanines*, 2001, **5**, 405-414, DOI: 10.1002/jpp.341.

63. T. M. Ziyadova, V. A. Burmistrov, V. E. Maizlish, and O. I. Koifman, *Kinet. Catal*., 2016, **57**, 313-318, DOI: 10.1134/S0023158416030186.

64. J. A. Goodwin, J. Agbo, J. Zuczek, A. Samuel, T. H. Aslund, L. R. Tuley, J. A. Simmons, R. J. Kimble, E. Magee, S. Creager, and J. Shetzline, *J. Porphyrins Phthalocyanines*, 2015, **19**, 1185-1196, DOI: 10.1142/S1088424615501023.

65. D. Etherbert, C. Yu, H. Imai, M. Ushio, S. Takeda, T. Naito, and T. Inabe, *Chem. Lett.*, 2006, **35**, 602-603, DOI: 10.1246/cl.2006.602.

66. Y. Ohtsuka, T. Naito, and T. Inabe, *J. Porphyrins Phthalocyanines*, 2005, **9**, 68-71, DOI: 10.1142/S1088424605000125.

67. T. Asari, T. Naito, T. Inabe, M. Matsuda, and H. Tajima, *Chem. Lett.*, 2004, **33**, 128-129, DOI: 10.1246/cl.2004.128.

68. P. A. Bernstein, and A. B. P. Lever, *Inorganica Chim. Acta*, 1992, **198-200**, 543-555, DOI: 10.1016/S0020-1693(00)92398-3.

69. C. Ercolani, A. M. Paoletti, G. Pennesi, and G. Rossi, *J. Chem. Soc., Dalton Trans.*, 1991, 1317-21, DOI: 10.1039/DT9910001317.

70. C. Hedtmann-Rein, M. Hanack, K. Peters, E. M. Peters, and H. G. Von Schnering, *Inorg. Chem.*, 1987, **26**, 2647-2651, DOI: 10.1021/ic00263a019.

71. H. Homborg, and W. Kalz, *Zeitschrift fuer Naturforschung, Teil B: Anorganische Chemie, Organische Chemie,* 1984, **39B**, 1490-1499.

72. N. V. Kondratenko, I. N. Tretyakova, E. A. Luk'yanets, S. V. Volkov, R. K. Orlova, V. N. Nemykin, and L. M. Yagupolskii, *Dyes and Pigments*, 1999, **41**, 101-109, DOI: 10.1016/S0143-7208(98)00066-7.

73. N. V. Kondratenko, V. N. Nemykin, E. A. Lukyanets, N. A. Kostromina, S. V. Volkov, and L. M. Yagupolskii, *J. Porphyrins Phthalocyanines*, 1997, **1**, 341-347, DOI: 10.1002/(SICI)1099-1409(199710)1:4<341::AID-JPP37>3.0.CO;2-K.

74. R. K. Al-Shewiki, S. Weheabby, N. Uhlig, M. Korb, T. Pester, S. Zahn, S. Grecchi, P. R. Mussini, T. Rueffer, and H. Lang, *Dalton Trans*, 2024, **53**, 3836-3854. DOI: 10.1039/D3DT03950A.

75. N. Tkachenko, V. Golovanov, A. Penni, S. Vesamaki, M. R. Ajayakumar, A. Muranaka, N. Kobayashi, and A. Efimov, *Phys. Chem. Chem. Phys.*, 2024, **26**, 18113-18128, DOI: 10.1039/D4CP01564A.

76. T. T. Tasso, T. Furuyama, and N. Kobayashi, *Inorg. Chem.*, 2013, **52**, 9206-9215, DOI: 10.1021/ic4002048.

77. A. Yazici, D. Ates, O. Bekaroglu, and N. Kobayashi, *J. Porphyrins Phthalocyanines*, 2006, **10**, 1140-1144, DOI: 10.1142/S1088424606000491.

78. N. Kobayashi, H. Miwa, and V. N. Nemykin, *J. Am. Chem. Soc.*, 2002, **124**, 8007-8020, DOI: 10.1021/ja0123812.

79. N. Kobayashi, H. Lam, W. A. Nevin, P. Janda, C. C. Leznoff, and A. B. P. Lever, *Inorg. Chem.*, 1990, **29**, 3415-3425, DOI: 10.1021/ic00343a028.

80. Z. Gasyna, N. Kobayashi, and M. J. Stillman, *J. Chem. Soc., Dalton Trans.*,1989, 2397-2405, DOI: 10.1039/DT9890002397.

81. D. V. Konarev, A.V. Kuzmin, S. S. Khasanov, and R. N. Lyubovskaya, *Dalton Trans*., 2013, **42**, 9870-9876, DOI: 10.1039/C3DT50855B.

82. H. Eckert, *Zeitschrift fuer Naturforschung, B: Chemical Sciences*, 1990, **45**, 1715-24, DOI: 10.1515/znb-1990-1219.

83. K. Kusuda, R. Ishihara, H. Yamaguchi, and I. Izumi, *Electrochim. Acta*, 1986, **31**, 657-663, DOI: 10.1016/0013-4686(86)87032-3.

84. H. Eckert, *Angewandte Chemie*, 1981, **93**, 216-18.

85. H. Eckert, and I. Ugi, *Angewandte Chemie*, 1975, **87**(23), 847.

86. F. Cariati, D. Galizzioli, F. Morazzoni, and C. Busetto, *J. Chem. Soc. Dalton Trans*., 1975, 556-561, DOI : 10.1039/DT9750000556.

87. F. Cariati, F. Morazzoni, and C. Busetto, *J. Chem. Soc. Dalton Trans.*, 1976, 496-500, DOI: 10.1039/DT9760000496.

88. G. Mercati, F. Morazzoni, M. Barzaghi, P. Carniti, V. Ragaini, and F. Campadelli, *J. Chem. Soc., Faraday Trans., 1*, 1979, **75**, 1857-67, DOI: 10.1039/F19797501857.

89. G. Mercati, and F. Morazzoni, *Inorg. Chim. Acta*, 1977, **25**, L115-L116, DOI: 10.1016/S0020-1693(00)95669-X.

90. A. B. P. Lever, S. R. Pickens, P. C. Minor, S. Licoccia, B. S. Ramaswamy, and K. Magnell, *J. Am. Chem. Soc.*, 1981, **103**, 6800-6806, DOI: 10.1021/ja00413a003.

91. M. G. Cory, and M. C. Zerner, *Chem. Rev.*,1991, **91**, 813-822, DOI: 10.1021/cr00005a009.

92. K. Murata, and K. Ishii, *Eur. J. Inorg. Chem.*, 2017, 5103-5107, DOI: 10.1002/ejic.201700668.

93. E. A. Ough, and M. J. Stillman, *Inorg. Chem.* 1995, **34**, 4317-4325, DOI: 10.1021/ic00121a009.

94. B. E. Muldowney, H. M. Grace, B. J. McNicholas, and V. N. Nemykin, *J. Porphyrins Phthalocyanines*, 2025, **29**, 110-122, DOI: 10.1142/S1088424625500038.

95. V. N. Nemykin, and E. A. Lukyanets, *ARKIVOC*, 2010, 136-208, DOI: 10.3998/ark.5550190.0011.104.

96. E. A. Luk'yanets, S. A. Mukhalenko, and E. I. Kovshev, *Zhurnal Obshchei Khimii*, 1971, **41**, 934-935.

97. S, A. Mikhalenko, S. A. Gladyr, and E. A. Luk'yanets, *Zhurnal Organicheskoi Khimii*, 1972, **8**, 341-343.

98. M. J. Stillman, and A. J. Thomson, *J. Chem. Soc., Faraday Trans. 2*, 1974, **70**, 790-804, DOI: 10.1039/F29747000790.

99. M. J. Stillman, and A. J. Thomson, *J. Chem. Soc., Faraday Trans. 2*, 1974, **70**, 805-814, DOI: 10.1039/F29747000805.

100. B. R. Schrage, W. Zhou, L. A. Harrison, D. E. Nevonen, J. R. Thompson, K. E. Prosser, C. J. Walsby, C. J. Ziegler, D. B. Leznoff, and V. N. Nemykin, *Inorg Chem*, 2022, **61**, 20177-20199, DOI: 10.1021/acs.inorgchem.2c03456.

101. V. V. Minin, G. M. Larin, Y. V. Rakitin, A. V. Rotov, V. M. Derkacheva, O. L. Kaliya, O. E. and A. Luk'yanets, *Zhurnal Neorganicheskoi Khimii*, 1987, **32**, 1135-1139.

102. Y. V. Rakitin, V. V. Minin, and G. M. Larin, *Koordinatsionnaya Khimiya*, 1988, **14**, 1090-1097.

103. S. Sievertsen, H. Grunewald, and H. Homborg, *Anorg. Allg. Chem.* 1993, **619**, 1729-1737.

104. J. M. Assour, and W. K. Kahn, *J. Am. Chem. Soc.*,1965, **87**, 207-212, DOI: 10.1021/ja01080a013.

105. R. Mason, G. A. Williams, and P. E. Fielding, *J. Chem. Soc., Dalton Trans.*, 1979, 676-683, DOI: 10.1039/DT9790000676.

106. H. Hueckstaedt, and H. Homborg, *Zeitschrift fuer Anorganische und Allgemeine Chemie*, 1998, **624**, 715-720.

107. M. Matsuda, T. Asari, T. Naito, T. Inabe, N. Hanasaki, and H. Tjima., *Bull. Chem. Soc. Jpn.*, 2003, **76**, 1935-1940, DOI: 10.1246/bcsj.76.1935.

108. M. Nishi, Y. Hayata, N. Hoshino, N. Hanasaki, T. Akutagawa, and M. Matsuda, *Dalton Trans.* 2019, 17723-17728, DOI: 10.1039/C9DT03653A.

109. T. Inabe, and Y. Maruyama, *Bull. Chem. Soc. Jpn.,* 1990, **63**, 2273-2280, DOI: 10.1246/bcsj.63.2273.

110. J. Janczak, and R. Kubiak, *Inorg. Chim. Acta*, 2003, **342**, 64-76, DOI : 10.1016/S0020-1693(02)01060-5.

111. F. Cariati, F. Morazzoni, and M. Zocchi, *J. Chem. Soc. Dalton Trans*. 1978, 1018-1024.

112. D. E. Nevonen, L. S. Ferch, B. R. Schrage, and V. N. Nemykin, *Inorg. Chem.,* 2022, **61**, 8250–8266, DOI: 10.1021/acs.inorgchem.2.c00721.

113. P. C. Minor, M. Gouterman, and A. B. P. Lever, *Inorg. Chem*., 1985, **24**, 1894-1900, DOI: 10.1021/ic00206a040.

114. B. R. Hollebone, and M. J. Stillman, *Chem. Phys. Lett.*, 1974, **29**, 284-286, DOI: 10.1016/0009-2614(74)85032-3.

115. B. R. Hollebone, and M. J. Stillman, *J. Chem. Soc., Faraday Trans. 2*, 1978, **74**, 2107-2127, DOI: 10.1039/F29787402107.

116. Z. Gasyna, N. Kobayashi, and M. J. Stillman, *J. Chem. Soc., Dalton Trans.*, 1989, 2397-2405, DOI: 10.1039/DT9890002397.

117. J. Mack, M. J. Stillman, and N. Kobayashi, *Coord. Chem. Rev.*, 2007, **251**, 429-453, DOI: 10.1016/j.ccr.2006.05.011.

118. V. N. Nemykin, B. R. Schrage, D. E. Nevonen, L. A. Harrison, K. M. E. Newman, V. K. Paidi, and J. van Lierop, *Inorg. Chem.*, 2023, **62**, 10203-10220, DOI: 10.1021/acs.inorg.chem.3c00897.

119. V. N. Nemykin, V. Y. Chernii, S. V. Volkov, N. I. Bundina, O. L. Kaliya, V. D. Li, and E. A. Lukyanets, *J. Porphyrins Phthalocyanines*, 1999, **3**, 87-98, DOI: 10.1002/(SICI)1099-1409(199902)3:2<87::AID-JPP108>3.0.CO;2-G.

120. N. Kobayashi, F. Furuya, and G. C. Yug, *J. Porphyrins Phthalocyanines*, 1999, **3**, 433-438, DOI: 10.1002/(SICI)1099-1049(199909/10)3:6/7<433::AID-JPP152>3.0.CO;2-J.

121. N. Kobayashi, F. Furuya, G. C. Yug, H. Wakita, M. Yokomizo, and N. Ishikawa, *Chem. Eur. J.*, 2002, **8**, 1474-1484, DOI: 10.1002/1521-3765(20020315)8:6<1474::AID-CHEM1474>3.0.CO;2-P.

122. Y. Asano, J. Sato, T. Furuyama, and N. Kobayashi, *Chem. Commun.*, 2012, **48**, 4365-4367, DOI: 10.1039/C2CC31264F.

123. N. Ishikawa, and Y. Kaizu, *Coord. Chem. Rev.* 2002, **226**, 93-101, DOI: 10.1016/S0010-8545(01)00439-8.

124. N. Ishikawa, and Y. Kaizu, *J. Porphyrins Phthalocyanines*, 1999, **3**, 514-521, DOI: 10.1002/(SICI)1099-1409(199908/10)3:6/7<514:;AID-JPP169>3.0.CO;2-U.

125. O. Ohno, N. Ishikawa, H. Matsuzawa, Y. Kaizu, and H. Kobayashi, *J. Phys. Chem.*, 1989, **93**, 1713-1718, DOI: 10.1021/j100342a010.

126. N. Ishikawa, O. Ohno, Y. Kaizu, and H. Kobayashi, *J. Phys. Chem.*, 1992, **96**, 8832-8839, DOI: 10.1021/j100201a028.

127. N. Ishikawa, and Y. Kaizu, *Chem. Phys. Lett.*, 1994, **228**, 625-632, DOI: 10.1016/0009-2614(94)00982-1.

128. N. Ishikawa, *J. Porphyrins Phthalocyanines*, 2001, **5**, 87-101, DOI: 10.1002/1099-1409(200101)5:1<87::AID-JPP304>3.0.CO;2-Q.

129. R. V., Belosludov, D. E. Nevonen, H. M. Rhoda, J. R. Sabin, and V. N. Nemykin, *J. Phys. Chem. A*, 2019, **123**, 132-152, DOI: 10.1021/acs.jpca.8b07647.

130. V. N. Nemykin, D. E. Nevonen, W. R. Osterloh, L. S. Ferch, L. A. Harrison, B. S. Marx, K. and M. Kadish, *Inorg. Chem.*, 2021, **60**, 16626-16644, DOI: 10.1021/acs.inorgchem.1c02520.

131. E. A. Ough, and M. J. Stillman, *Inorg. Chem.*, 1994, **33**, 573-583, DOI: 10.1021/ic00081a028.

132. M. Gouterman, *J. Chem. Phys.*, 1959, **30**, 1139-1161, DOI: 10.1063/1.1730148.

133. M. Gouterman, *J. Mol. Spectr.*, 1961, **6**, 138-163, DOI: 10.1016/0022-2852(61)90236-3.

134. M. Gouterman, G. Wagniere, and L. C. Snyder, *J. Mol. Spectr.*, 1963, **11**, 108-127, DOI: 10.1016/0022-2852(63)90011-0.

135. A. B. P. Lever, *Inorganic Electronic Spectroscopy (Second Edition)*, Elsevier, New York, 1984.

136. Y. Nishida, and S. Kida, *Bull. Chem. Soc. Jpn.*, 1972, **45**, 461-465, DOI: 10.1246/bcsj.45.461.

137. T. Zhnag, I. E. Brumboiu, V. Lanzilotto, J. Lüder, C. Grazioli, E. Giangrisostomi, R. Ovsyannikov, Y. Sassam I. Bidermane, M. Stupar, M. de Simone, M. Coreno, B. Ressel, M. Pedio, P. Rudolf, B. Brena, and C. Puglia, *J. Phys. Chem. C*, 2017, **121**, 26372-26378, DOI: 10.1021/acs.jpcc.7b08524.

138. P. Krüger, *Radiation Phys. Chem.*, 2020, **175**, 108051, DOI: 10.1016/j.radphyschem.2018.11.005.

139. E. I. Solomon, and A.B.P. Lever, *Inorganic Electronic Structure and Spectroscopy, Vol. 1*, Wiley, 1999, New York, pp. 93-159.

140. Y. Nishida, K. Ida, and S. Kida, *Inorg. Chim. Acta*, 1980, **38**, 113-116, DOI: 10.1016/S0020-1693(00)91944-3.

141. L. M. Engelhardt, and M. J. Green, *J. Chem. Soc. Dalton Trans*, 1972, 724-728, DOI: 10.1039/DT9720000724.

142. R. G. Hadt, V. N. Nemykin, J. G. Olsen, and P. Basu, Phys. Chem. Chem. Phys., 2009, **11**, 10377-10384, DOI: 10.1039/B905554A.

143. V. N. Nemykin, and P. Basu, *Inorg. Chem.*, 2003, **42**, 4046-4056, DOI: 10.1021/ic0262942.s001.

144. Origin(Pro), Version 2025b. OriginLab Corporation, Northampton, MA, USA.

145. Gaussian 16, Revision B.01, Frisch MJ, Trucks DW, Schlegel HB, Scuseria GE, Robb MA, Cheeseman JR, Scalmani G, Barone V, Petersson GA, Nakatsuji H, Li X, Caricato M, Marenich A,

Bloino J, Janesko BG, Gomperts R, Mennucci B, Hratchian HP, Ortiz JV, Izmaylov AF, Sonnenberg JL, Williams-Young D, Ding F, Lipparini F, Egidi F, Goings J, Peng B, Petrone A, Henderson T, Ranasinghe D, Zakrzewski VG, Gao J, Rega N, Zheng G, LiangW, Hada M, Ehara M, Toyota K, Fukuda R, Hasegawa J, Ishida M, Nakajima T, Honda Y, Kitao O, Nakai H, Vreven T, Throssell K, Montgomery Jr. JA, Peralta JE, Ogliaro F, Bearpark M, Heyd JJ, Brothers E, Kudin KN, Staroverov VN, Keith T, Kobayashi R, Normand J, Raghavachari K, Rendell A, Burant JC, Iyengar SS, Tomasi J, Cossi M, Millam JM, Klene M, Adamo C, Cammi R, Ochterski JW, Martin RL, Morokuma K, Farkas O, Foresman JB, and Fox DJ, Gaussian, Inc., Wallingford CT, 2016.

146 J. M. Tao, J. P. Perdew, V. N. Staroverov, and G. E. Scuseria, *Phys. Rev. Lett.*, 2003, **91**, 146401/1-146401/4, DOI: 10.1103/PhysRevLett.91.146401.

147. V. N. Staroverov, G. N. Scuseria, J. Tao, and J. P. Perdew, *J. Chem. Phys*., 2003, **119**, 12129-12137, DOI: 10.1063.1.1626543.

148. A. J. H. Wachters, *J. Chem. Phys*., 1970, **50**, 1033-1036, DOI: 10.1063/1.1673095.

149. A. D. McLean, and G. S. Chandler, *J. Chem. Phys*., 1980, **72**, 5639-5648, DOI: 10.1063/1.438980.

150. J. Tomasi, B. Mennucci, and R. Cammi, *Chem. Rev.*, 2005, **105**, 2999-3094, DOI: 10.1021/cr9904009.

151. A. L. Tenderholt, QMForge, version 2.1; Stanford University, CA, 2011. https://qmforge.net/.

Additional data are available on request from the corresponding authors.